Molecular basis of the activity and the regulation of the eukaryotic-like S/T protein kinase PknG from Mycobacterium tuberculosis

María-Natalia Lisa, Magdalena Gil, Gwenaëlle André-Leroux, Nathalie Barilone, Rosario Durán, Ricardo Biondi, Pedro M. Alzari

Structure

Molecular basis of the activity and the regulation of the eukaryotic-like S/T protein kinase PknG from Mycobacterium tuberculosis

--Manuscript Draft--

Manuscript Number:	STRUCTURE-D-15-00082R
Full Title:	Molecular basis of the activity and the regulation of the eukaryotic-like S/T protein kinase PknG from Mycobacterium tuberculosis
Article Type:	Research Article
Keywords:	PknG; S/T protein kinase; kinase regulation; rubredoxin; tetratricopeptide repeats (TPR); tuberculosis
Corresponding Author:	Pedro M. Alzari, PhD Institut Pasteur Paris, FRANCE
First Author:	María-Natalia Lisa
Order of Authors:	María-Natalia Lisa
	Magdalena Gil
	Gwénaëlle André-Leroux
	Nathalie Barilone
	Rosario Durán
	Ricardo M. Biondi
	Pedro M. Alzari, PhD
Abstract:	Tuberculosis remains one of the world's deadliest human diseases, with a high prevalence of antibiotic resistant Mycobacterium tuberculosis (Mtb) strains. A molecular understanding of processes underlying regulation/adaptation of bacterial physiology may provide novel avenues for the development of antibiotics with unconventional modes of action. Here we focus on the multidomain S/T protein kinase PknG, a soluble enzyme that controls central metabolism in Actinobacteria and has been linked to Mtb infectivity. Our biochemical and structural studies reveal how different motifs/domains flanking the catalytic core regulate substrate selectivity without significantly affecting the intrinsic kinase activity, whereas a rubredoxin-like domain is shown to downregulate catalysis through specific intramolecular interactions that modulate access to a profound substrate-binding site. Our findings provide the basis for the selective and specific inhibition of PknG and open new questions about regulation of related bacterial and eukaryotic protein kinases.

Institut Pasteur

Paris, le 01/04/15

Manuscript: STRUCTURE-D-15-00082

Title: Molecular basis of the activity and the regulation of the eukaryotic-like S/T protein kinase PknG from *Mycobacterium tuberculosis*

Dear Editor,

Please find enclosed the revised version of our manuscript, in which we have taken into account the questions and remarks of the reviewers. In an accompanying file, we submit a point by point answer to the reviewer's comments.

With my best regards,

Prof. Pedro M. Alzari

Institut Pasteur
25-28 rue du Docteur Roux
75724 Paris Cedex 15

Reviewer 1:

The authors study the regulation and structure of the mycobacterial Ser/Thr-kinase PknG. Enzymatic assays show an important positive role of N-terminal autophosphorylation sites for docking by an FHA-containing substrate protein, as well as an autoinhibitory role of the Rdx domain that is located N-terminal to the kinase domain. Two high resolution crystal structures of Rdx-kinase domain units of PknG were solved in complex with ADP and ATP-gammaS, respectively. Analysis of the structures in conjunction with additional enzymatic assays defined an extended peptide substrate binding groove and indicated that PknG kinase activity may not depend on the conserved K-E salt bridge between the N-lobe beta sheets and the alpha C helix.

Overall, this is a highly interesting paper that presents conclusive evidence for the above-described mechanisms using structural and biochemical/biophysical methods. The manuscript is clearly written, was easy for me to follow and a pleasure to read. The reported findings are very interesting and novel in terms of structural mechanisms of kinase regulation and in comparison to kinase-substrate relations in eukaryotic protein kinases.

Still, there are a few comments that need to be addressed:

1. The authors should present a coomassie stained gel with the 5 purified PknG constructs that are used for the assays in figure 1a/b to be able to judge purity and possible degradation/stability of the proteins. The figure legends need to list the number of replicates and if error bars represent SD or SEM.

Answer: A Coomassie-stained SDS-PAGE of the deletion mutants has now been included in the revised Figure 1 as suggested.

2. It would be important to report if the purified proteins are unphosphorylated or already autophosphorylated on N-terminal Thr residues that were described to be important for GarA docking. If the proteins were not autophosphorylated, do the authors have an idea about the autophosphorylation kinetic as compared to substrate phosphorylation?

Answer: As we reported in our previous work on PknG (O'Hare et al, 2008, reference 11 in this manuscript), mass spectrometry (MS) analysis showed that recombinant PknG purified from *E. coli* is partially and heterogeneously phosphorylated within its N-terminal extension. In different

preparations, we repeatedly detected unphosphorylated, mono- and diphosphorylated protein species in up to four different phosphorylation sites, which renders very difficult to carry out meaningful enzyme kinetics. After 20 min incubation in the presence of ATP, PknG was found fully phosphorylated, and the results shown in Supplementary Figure 1c in the present manuscript are in good agreement with those previous findings. Even though these data give a general idea about the kinetics of PknG autophosphorylation, we cannot directly compare these results with GarA phosphorylation (which has a single phosphorylation site), as there is no reason to assume that the different sites in the N-terminal segment of PknG are phosphorylared with similar efficiencies or even *via* the same mechanism.

3. Page 9: A more detailed description of the Rdx-N-lobe interface should be added to the text (buried surface area, which key residues/sec. structure elements are involved etc).

Answer: This has been done in the revised version of the manuscript (page 10, first paragraph).

4. Page 11, first paragraph: A comparison with the ATP binding site of ePKs would help the reader to better understand differences and commonalities to the ATP-binding site of PknG.

Answer: A more detailed description taking into account this suggestion has now been included in the revised version of the manuscript (page 11, first paragraph).

5. Page 13: It is not clear to me why the results of the E198A mutation on PknG kinase activity are not reported as part of a figure or a table, but only mentioned in the text? As this piece of data results in a central conclusion of the paper, this needs to be changed.

Answer: Following the suggestion of the reviewer, the kinase activity of mutant $PknG_{E198A}$ has now been included in new Figure 5.

Reviewer 2:

The authors investigate the regulation of the most original bacterial eSTPK-like protein. Not only this is the sole cytoplasmic one among the M. tuberculosis protein kinases, but two extra domains also flank the catalytic domain. Those domains influences on the protein function remained poorly study despite the protein being a confirmed target for antibiotics development.

The paper is not the most original one, but the experimental data are strong and the new insights brought into the STPK biology, not only in the bacterial field but also for the eukaryotic homologues are sound.

They first shown with two PknG substrate GarA, a FHA containing domain protein, and a peptide derived from the phosphorylation site (17-mer) that both Nter/Rdx and TPR domain are important for the substrate specificity/recruitment but not for the kinase activity. Then they show that the Rdx domain deletion leads to an activity increase for both substrates compared to the sole deletion of the 73 first residues. Then they solve a new PknG X-ray structure in complex with ADP or gamma-S-ATP in a new open-form conformation and with different domain interactions compare to the already solved structure. The analysis or the new and old structures allows to better understand the possible ligand positioning, the role of the Rdx domain (a very nice analysis) and also to better characterize an original feature, the absence of the conserved salt bridge Glu-Lys within the catalytic domain. This feature was known but is here better characterized.

Overall the paper brings a much detailed PknG characterization and the new structure display some complex interaction between the Rdx and kinase domains that not only influence the ligand entrance but also the positioning and most certainly the dynamic of key catalytic residues.

Proposed corrections:

"Major" points:

The authors show that PknG is more active on the GarA protein compared to a 17mer peptide derivate from this protein. The authors postulate that the gain in activity was mostly due to the binding of the FHA domain of GarA to the N-terminal domain of PknG. When the PknG 73 N-terminal residues are deleted the activity dropped for GarA but not for the peptide, confirming the hypothesis that N-terminal phosphorylations are important for the substrates

recruitment in the case of a FHA containing protein. The new structure shows that the Rdx domain down-regulate the kinase activity, but when this domain is deleted there is indeed an increase of the kinase activity in the case of the 17-mer compared to the WT PknG, but that's not the case in the case of GarA where the activity dropped. This is puzzling….

Answer: Indeed, the results are consistent. It should be noted that the differences observed between WT PknG and $PknG_{\Delta 137}$ on full-length GarA are due to two distinct factors, namely (1) the presence or absence of the phosphorylated docking sites in the N-terminus and (2) the presence or absence of the Rdx domain. The observation that the activity dropped for $PknG_{\Delta 137}$ on GarA (compared to WT PknG, as noted by the reviewer) thus implies that the (negative) effect of missing the phosphorylation docking sites dominates over the (positive) effect of removing the Rdx domain. On the other hand, to assess **only** the effect of deleting Rdx, one should compare the activities of $PknG_{\Delta 73}$ and $PknG_{\Delta 137}$ on GarA. Clearly, in this case the deletion of Rdx increased the kinase activity on GarA, in a similar way as observed on the peptide substrate. We have now added a sentence to clarify this point in the revised version of the manuscript (page 9, lines 180-181).

There are some issues with the enzymology data reported in the paper. The Km value is missing for GarA. Could not find it in the reference 11 and 12. At 25µM we are not sure we are at saturation as we can see that we are not at 330µM for the 17-mer. Would have been nice to have an equivalent figure as S1 for GarA (specific activity various GarA concentration). The issue here is to compare specific activity for two ligands at different concentration in non-saturating conditions. To my knowledge it is better to use kcat/Km (value given for the 17mer but not for GarA) or even better to compare kcat and Km. Also the conclusion drown line 134 seems a bit overstated regarding the data with no affinity measure here (even so the authors are certainly right).

Answer: We have not re-calculated the Km for GarA phosphorylation by PknG, since it has been reported to be 2.1 µM (Tiwari *et al*, 2009). Thus, it is safe to assume that saturation is achieved at 25 µM GarA, as employed in our activity measurements. We have now included this reference in the revised version of the manuscript (pages 6/7, lines 130-133).

Line 405: The authors mention with reason that in previous study "the structural integrity of those PknG mutants was not opportunely assessed". Unfortunately in this study as well mutant characterizations seem to be also missing.

Answer: In this work, we have crystallized the PknG mutant having the lowest activity against GarA ($PknG_{\Delta 73,\Delta TPR}$) and showed it to have the same overall structure that the equivalent domains in the wild-type enzyme (PDB code 2PZI), clearly indicating that the mutation is not affecting the structural integrity of the protein. All other PknG mutants described in our work retain at least a wild-type-comparable activity against the 17-mer peptide substrate, supporting the notion that the structural integrity was not affected by the mutations. In contrast, the authors of the previous study reported a loss of function due to the Cys mutation(s) in the Rdx domain, which they attributed to the essentiality of the Rdx domain but which could alternatively be due to structural disruption of the metal center.

Minor points:

- From line 175, if the authors mentioned the domain delimitation of the structure they solved the domain delimitation of the 2007 structure is not mentioned. That would be useful so understand what we are comparing in the text.

Answer: The domain delimitation used in our work is indeed derived from the 2007 structure and sequence analysis. As far as we can see, there are no contradictions in this regard between the two works. Concerning the crystal structures that we compare in the text, the one reported in the previous work (PDB code 2PZI) corresponds to $PknG_{\Delta 73}$ in complex with an inhibitor, whereas we report here the structure of $PknG_{\Delta 73,\Delta TPR}$ in complex with nucleotides.

-Is the Rdx position shift in the new structure compare to the older one (2PZI) due to the nature of the ligand, the new protein delimitation, or crystallogenesis?

Answer: The shift in the position of the Rdx domain with respect to the catalytic domain may be due, at least in part, to the presence of different ligands in the kinase active site (as discussed in the main text of the manuscript), as well as to distinct effects of crystal packing. In contrast, the observed differences are certainly not due to the use of different constructs.

-With the 17-mer peptide, the specific activity is 1.9 +/- 0.1 x10-5 nmol/µM2.min, so at 330 µM a 0.0063 nmol/µM.min specific activity is expected, but the data in Fig. 1B seems to indicate 0.0046.

Answer: These values have been determined in independent experiments (see details in the Experimental Procedures section) and, taking into account the experimental errors affecting these experiments, they are in relatively good agreement.

Graphical Abstract

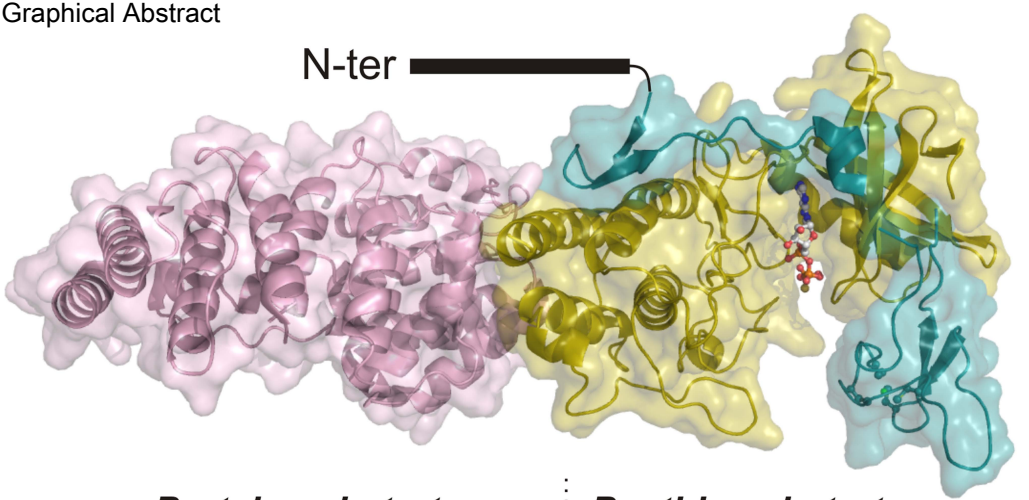

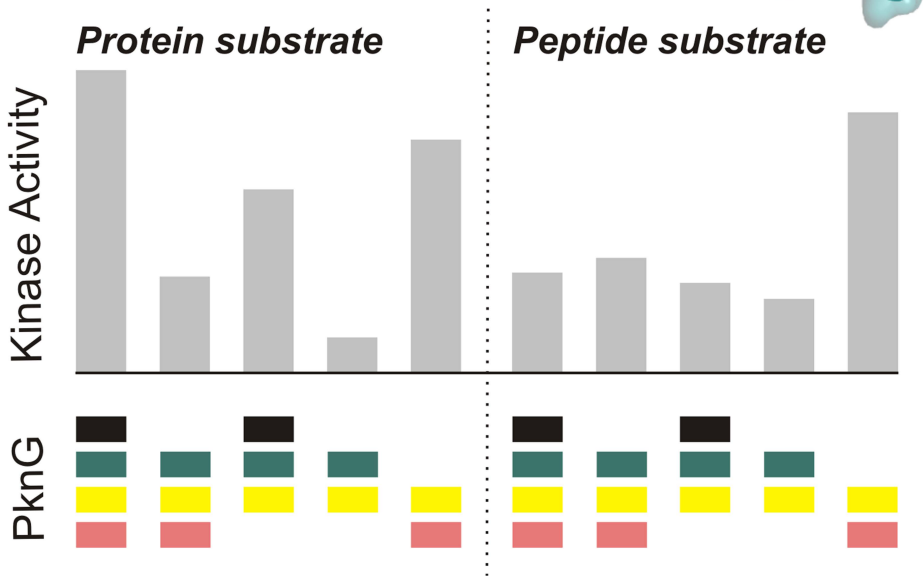

Molecular basis of the activity and the regulation of the eukaryotic-like S/T protein kinase PknG from *Mycobacterium tuberculosis*

María-Natalia Lisa [1,2,3], Magdalena Gil [4], Gwénaëlle André-Leroux [1,2,3,5], Nathalie Barilone [1,2,3,6], Rosario Durán [4], Ricardo M. Biondi [7] and Pedro M. Alzari [1,2,3,*]

[1] *Institut Pasteur, Unité de Microbiologie Structurale, 25 rue du Docteur Roux, 75724 Paris, France*

[2] *CNRS UMR 3528 'Biologie structurale des processus cellulaires et maladies infectieuses', Institut Pasteur, Paris, France,*

[3] *Université Paris Diderot, Sorbonne Paris Cité, Microbiologie structurale, Paris Cedex 15, France*

[4] *Unidad de Bioquímica y Proteómica Analíticas, Instituto de Investigaciones Biológicas Clemente Estable e Institut Pasteur de Montevideo, Mataojo 2020, Montevideo, 11400, Uruguay*

[5] *INRA, UR1404 Unité Mathématiques et Informatique Appliquées du Génome à l'Environnement, F78352 Jouy-en-Josas, France*

[6] *Current address: Institut Pasteur, Unité de Neuro-Immunologie viral, 25 rue du Dr. Roux, 75724 Paris Cedex 15, France*

[7] *Research Group PhosphoSites, Medizinische Klinik 1, Universitätsklinicum Frankfurt, Theodor-Stern-Kai 7, 60590 Frankfurt*

[*] To whom correspondence should be addressed: PMA (pedro.alzari@pasteur.fr), Unité de Microbiologie Structurale, 25 rue du Dr. Roux, 75724 Paris Cedex 15, France. Fax: +33-1-45688604

SUMMARY

Tuberculosis remains one of the world's deadliest human diseases, with a high prevalence of antibiotic resistant *Mycobacterium tuberculosis* (*Mtb*) strains. A molecular understanding of processes underlying regulation/adaptation of bacterial physiology may provide novel avenues for the development of antibiotics with unconventional modes of action. Here we focus on the multidomain S/T protein kinase PknG, a soluble enzyme that controls central metabolism in Actinobacteria and has been linked to *Mtb* infectivity. Our biochemical and structural studies reveal how different motifs/domains flanking the catalytic core regulate substrate selectivity without significantly affecting the intrinsic kinase activity, whereas a rubredoxin-like domain is shown to downregulate catalysis through specific intramolecular interactions that modulate access to a profound substrate-binding site. Our findings provide the basis for the selective and specific inhibition of PknG and open new questions about regulation of related bacterial and eukaryotic protein kinases.

INTRODUCTION

Reversible protein phosphorylation has evolved as a ubiquitous molecular mechanism of protein regulation. In eukaryotes, protein phosphorylation commonly takes place on serine, threonine and tyrosine residues and is catalyzed by a large group of enzymes, the eukaryotic protein kinases (ePKs) (Huse and Kuriyan, 2002; Kornev and Taylor, 2010). Evolutionary related S/T protein kinases (STPKs) also exist in many sequenced bacterial genomes, including important human pathogens such as *Mycobacterium tuberculosis* (*Mtb*), *Staphylococcus aureus*, *Pseudomonas aeruginosa* and *Bacillus anthracis*, where they fulfill important roles in bacterial physiology and pathogenesis (Wehenkel et al., 2008). While kinase mediated signaling mechanisms in bacteria share important common features with their eukaryotic counterparts, specific differences are emerging as novel functions and components of bacterial phosphosystems are being identified (Sherman and Grundner, 2014). The genome of *Mtb*, the causative agent of tuberculosis, codes for eleven STPKs (Cole et al., 1998), some of which have been extensively investigated and shown to be either essential for and/or involved in the regulation of metabolic processes, gene transcription, cell division and host-pathogen interactions (Wehenkel et al., 2008; Av-Gay and Everett, 2000; Sassetti et al., 2003). Among these, the protein kinase PknG is exclusively found in Actinobacteria and displays a unique modular organization, which seems to be absent in known ePKs.

PknG is of particular interest because of its roles in *Mtb* pathogenicity, where it has been proposed to inhibit the phagosome-lysosome fusion within the infected macrophage (Walburger et al., 2004), and in bacterial metabolism, where it regulates the fate of α-ketoglutarate, a key metabolic intermediate at the crossroads of the

tricarboxylic acid cycle (C metabolism) and glutamate synthesis (N metabolism) (Cowley et al., 2004; Ventura et al., 2013). While the signaling pathway mediating infectivity has not been unequivocally determined, PknG is known to phosphorylate *in vivo* the *Mtb* regulator GarA (O'Hare et al., 2008), a FHA (Forkhead Associated) protein (England et al., 2009; Barthe et al., 2009) that controls the accumulation of glutamate by direct binding to three metabolic enzymes that use α-ketoglutarate as substrate (O'Hare et al., 2008; Nott et al., 2009). Thus, while the knock down of GarA induces a glutamate/glutamine/asparagine auxotropy (these aminoacids are required as N donors) (Ventura et al., 2013), *Mtb* ΔPknG shows increased levels of intracellular glutamate (Cowley et al., 2004) and the related *Corynebacterium glutamicum* ΔPknG cannot grow in a minimal medium containing glutamine as the sole C source (Niebisch et al., 2006).

Despite these dual roles in bacterial physiology and pathogenesis, very little is known about the molecular basis of PknG activity and regulation. PknG is a multidomain protein, with a unique domain organization. Flanking the kinase catalytic core, the protein contains a possibly unstructured N-terminal extension, a rubredoxin (Rdx)-like domain immediately adjacent to the catalytic core and a C-terminal dimerization domain composed of tetratricopeptide repeats (TPR) (Scherr et al., 2007) (Fig. 1A). In contrast to most other *Mtb* kinases (Duran et al., 2005; Prisic et al., 2010), the activation loop (and the entire catalytic domain) of PknG is not phosphorylated on serine or threonine residues. Instead, four autophosphorylation sites (T_{23}, T_{32}, T_{63} and T_{64}) were identified within the N-terminal extension of the protein (O'Hare et al., 2008; Scherr et al., 2009; Prisic et al., 2010), where they provide pT-dependent anchoring sites for high affinity interactions with the FHA domain of GarA (O'Hare et al., 2008).

The Rdx domain contains the two characteristic CxxCG motifs in which the cysteine residues act as ligands of a divalent metal ion (Scherr et al., 2007), and is tightly associated with the small lobe of the kinase domain, giving rise to a deep substrate-binding cleft. This metal binding ability and the absence of pT residues in the activation loop led some authors to suggest a possible redox-dependent regulation mechanism of PknG (Scherr et al., 2007; Tiwari et al., 2009; Gil et al., 2013; Chao et al., 2010), but no strong evidence is available in support of this hypothesis and the underlying mechanisms involved are yet to be elucidated.

Here we investigate the molecular mechanisms of PknG regulation by its N-terminal region, the C-terminal TPR domain, and the helix αC, which act jointly in determining the selective phosphorylation of the physiological substrate GarA, together with the molecular details for the inhibition of PknG activity by the Rdx domain. Furthermore, we have found that PknG interacts with an extended peptide sequence at the protein substrate binding site, but that, contrary to the knowledge about ePKs (Huse and Kuriyan, 2002; Kornev and Taylor, 2010), the highly conserved salt bridge between a lysine side-chain that coordinates the α and β phosphates of ATP and a glutamate residue from helix αC is not essential for the kinase activity. Altogether, the protein kinase PknG from *Mtb* represents a detailed example regarding molecular determinants of activity, interaction with the substrates and mechanism of regulation within the family of STPKs, providing alternatives for the design of selective inhibitors with potential therapeutic applications.

RESULTS

PknG domains flanking the catalytic core contribute to the selective phosphorylation of GarA

Full-length PknG from *Mycobacterium tuberculosis* displays a unique multi-domain organization, containing a possibly unstructured N-terminal extension (residues 1-98), a rubredoxin (Rbx)-like domain (residues 99-137), the kinase catalytic core (residues 138-405) and a C-terminal tetratricopeptide repeat (TPR) domain (residues 406-750) (Fig. 1A). To understand the roles of these flanking regions in modulating PknG kinase activity, we first measured the specific activity of PknG against two different substrates: (a) the small protein GarA, a physiological substrate of PknG containing a FHA domain with high affinity for phosphorylated threonine residues (O'Hare et al., 2008; England et al., 2009) (Fig. 1B, left panel), and (b) a 17-mer peptide (SDEVTVET$_{21}$TSVFRADFL) derived from GarA (residues 14-30), centered around the phosphorylatable T_{21} (O'Hare et al., 2008) and lacking the FHA domain, to serve as a reporter of the intrinsic activity of the PknG catalytic domain (Fig. 1B, right panel). The kinase activity of full-length PknG varied linearly with the concentration of the 17-mer peptide up to 1 mM (Fig. S1A), indicating a high K_M (> 1 mM) and the slope (k_{cat}/K_M) providing a measure of the catalytic efficiency for this substrate ((1.9 $\pm$ 0.1) 10^{-5} nmol/μM^2.min). As a comparison, the phosphorylation of GarA by wild type PknG was approximately three times higher than for the 17-mer substrate even though a *ca.* 15 times lower concentration of GarA was used (Fig. 1B), indicating a 45-fold higher activity towards GarA due to the selective docking interaction granted by the FHA domain. Furthermore, when taking into account the K_M value of 2.1 µM previously reported for GarA phosphorylation by

PknG (Tiwari et al., 2009), the catalytic efficiency would be ~0.007 nmol/μM^2.min, *ca.* 400 times higher than that estimated for the 17-mer peptide substrate.

We then tested the selectivity of GarA phosphorylation by a PknG deletion mutant lacking the N-terminal autophosphorylated threonines (PknG$_{\Delta 73}$) (O'Hare et al., 2008). This mutant presented a *ca.* three times lower kinase activity against GarA compared to the wild type enzyme, while phosphorylation of the 17-mer peptide was unaffected (Fig. 1B). Thus, these results indicated that segment 1-73, including all PknG pT sites (O'Hare et al., 2008; Scherr et al., 2009), had no effect on the intrinsic activity of the kinase domain but was an important determinant of the kinase affinity and specificity towards its physiological substrate GarA. In line with this observation, PknG ability to phosphorylate the 17-mer peptide remained unaffected after addition of the isolated FHA domain of GarA (Fig. S1B), indicating that the activity of PknG is not modulated by interactions of the N-terminal pT residue(s) with the FHA domain. It should be noted, however, that the moderate decrease in GarA phosphorylation due to PknG mutation Δ73 did not fully explain the much larger difference observed between the phosphorylation of GarA and the 17-mer peptide by full-length PknG, suggesting that additional motifs may also contribute to GarA selectivity.

We therefore investigated the effect of the C-terminal TPR domain on PknG kinase activity. Interestingly, both phosphorylation of the 17-mer peptide as well as PknG autophosphorylation remained unchanged upon removal of the C-terminal region 406-750, encompassing a linker and the TPR domain (mutant PknG$_{\Delta TPR}$) (Fig. 1B and Fig. S1C). In contrast, the kinase activity of PknG$_{\Delta TPR}$ against GarA was lower than that of the wild type enzyme. Altogether, these results indicated that the TPR domain

did not affect the intrinsic kinase activity of PknG but that it contributed to the specific phosphorylation of the physiological substrate GarA.

The available crystal structure of PknG (PDB code 2PZI, comprising residues 74-750) suggested a role of the TPR domains in protein dimerization (Scherr et al., 2007). However, our analytical ultracentrifugation experiments (Fig. S1D) indicated that full-length PknG behaves mainly as a monomer in solution (70%) even at high protein concentration (1 mg/ml). It is therefore unclear how the TPR domain could exert the observed modulation of PknG activity. To further investigate this issue, we studied a PknG deletion mutant lacking both the first 73 N-terminal residues as well as the whole C-terminal TPR domain ($PknG_{\Delta 73,\Delta TPR}$). Notably, the kinase activity of $PknG_{\Delta 73,\Delta TPR}$ towards the 17-mer peptide resulted similar to those of the wild type enzyme, $PknG_{\Delta 73}$ and $PknG_{\Delta TPR}$ (Fig. 1B), whereas the phosphorylation of GarA was still further reduced in comparison with $PknG_{\Delta 73}$ and $PknG_{\Delta TPR}$. This indicated a cumulative effect of both PknG regions on substrate selectivity and suggested that the role of the TPR domain was independent of the pT-dependent interactions between the kinase and the FHA domain of GarA.

The Rdx domain downregulates the kinase activity of PknG

While all known bacterial PknG orthologs conserve the N-terminal region and the TPR domain, the Rdx domain is present only in PknGs within few suborders of the *Actinomycetales*, including the genus *Streptomyces* and *Mycobacterium* (Gil et al., 2013). Interestingly, while the deletion of the N-terminal extension and/or the TPR domain did not influence the intrinsic kinase activity of PknG against the 17-mer peptide, deletion of the Rdx domain (mutant $PknG_{\Delta 137}$) promoted a significantly higher

activity against the peptide substrate (Fig. 1B), clearly evidencing a release of an inhibition of PknG activity mediated by the Rdx domain. Consistent with this, $PknG_{\Delta 137}$ showed a *ca.* 2.5 times higher activity than $PknG_{\Delta 73}$ against GarA (Fig. 1B).

To further investigate the molecular basis of this regulatory process, we determined the high-resolution crystal structures of $PknG_{\Delta 73,\Delta TPR}$ in complex with either ADP or ATPγS respectively to 1.74 Å and 1.9 Å resolutions (Table 1). The final atomic models comprise PknG residues 83-404, including a fragment of the N-terminal segment, the Rdx domain and the kinase catalytic core. In both structures, *mFo–DFc* sigma-A-weighted electron density maps clearly revealed the bound nucleotide and two Mg(II) cations at the active site as well as one cation identified as a Zn(II) ion (Fig. S2) coordinated by residues C_{106}, C_{109}, C_{128} and C_{131} in the Rdx domain. The close association between the Rdx domain and the N-lobe of the catalytic core (Fig. 2A) generates a much deeper substrate binding cleft as compared to other Hank-type protein kinases, suggesting that the active site of PknG could selectively bind extended peptide substrates. When comparing the available PknG crystal structures (Fig. 2A) important differences in the position of the Rdx domain become apparent. In particular, the Rdx domain can adopt different positions in front of the active site of PknG, interacting or not with the kinase C-lobe, without affecting overall kinase fold and topology. Differences between the open and closed states in the different crystal structures are not due to conformational changes in the Rdx domain itself as a RMSD of only 0.31 Å is found among 34 alpha carbons in segment 99-137. Instead, a hinge motion takes place involving residues 200-205, 210-213 and 236-237 in the kinase domain, leaving a more open active site in the structures of $PknG_{\Delta 73,\Delta TPR}$, more permissive for substrate binding (Fig. 2A).

In available PknG crystal structures, the interface area between the Rdx domain and the kinase catalytic core spans 300-350 $Å^2$, and there is a conserved hydrogen bond between the carbonyl oxygen of residue F_{137} and the side chain of W_{164} (sequence adjacent to the G-rich loop, in the β_2 strand). Besides, in the crystal structures of $PknG_{\Delta 73,\Delta TPR}$, the Rdx domain contacts the kinase catalytic core through the ionic interaction between the conserved residues E_{125} and H_{223} (Fig. 2B, left panel). Residue H_{223} is located in the loop connecting the β_4 and β_5 strands in the kinase N-lobe. This loop is particularly long in PknG orthologs containing a Rdx domain (Fig. S3), suggesting that the entire region may be functionally relevant. Interestingly, in model 2PZI (Scherr et al., 2007), where the Rdx domain approaches the kinase C-lobe and occludes the active site (Fig. 2A, right panel), residues E_{125} and H_{223} are distant from each other and do not interact (Fig. 2B, right panel), indicating that these residues may contribute to regulate the position of the Rdx domain. Another contact with the kinase N-lobe involves the stacking of the conserved W_{107} (sequence adjacent to the metal ligand C_{106}) and H_{185} (in the loop connecting the β_3 strand and the αC helix) (Fig. 2B). These motifs harbor the catalytically relevant residues K_{181} (K_{72} in the ePK PKA) and E_{198} (E_{91} in PKA), respectively. Besides, the $N_{\varepsilon 2}$ atom of H_{185} hydrogen bonds the carbonyl oxygen of residue G_{161} in the kinase G-rich loop (Fig. 2B and next section), involved in positioning the ATP phosphates within the kinase active site. Thus, the PknG Rdx domain not only restricts the substrate entrance into the active site but also links catalytically relevant structural motifs within the kinase core. These observations therefore provide a structural framework to explain the regulation of the intrinsic kinase activity of PknG by the Rdx domain.

The ATP binding site of PknG

Most PknG residues within the ATP binding site regions (as defined by Traxler and Furet, 1999) are functionally conserved and adopt conformations very similar to those observed for PKA and other ePKs. Thus, the adenine moiety is buried in a hydrophobic pocket and makes two direct hydrogen bond interactions with the enzyme: the amine N at position 6 binds the backbone carbonyl oxygen of E_{233}, and the N_1 atom binds the amide of V_{235} (Fig. 3, left panel). Besides, the N_7 atom establishes a water-mediated interaction with the amide of D_{293}. Additional indirect contacts take place between the nucleoside and the protein: two water molecules link the adenine N_3 atom, the ribose O_2* position and the backbone carbonyl oxygens of V_{235} and G_{237}, and other water molecule contacts both the ribose O_2* and 0_3* atoms and the amide of S_{239}. Besides, van der Waals contacts are made with the side chains of I_{157}, A_{158}, I_{165}, V_{179}, V_{211}, M_{232}, Y_{234}, V_{235}, M_{283}, and I_{292}. Most PknG residues that bind the inhibitor AX20017 in 2PZI (Scherr et al., 2007) are also involved in nucleotide binding, except for I_{87}, A_{92} and G_{236} that interact with the cyclopropyl ring of the molecule.

The G-rich motif (A_{158}HGGLGW) within the N-lobe of PknG kinase domain acts as a flap that covers the nucleotide (Fig. 3, right panel). The main chain amides of G_{161} and L_{162} hydrogen bonds the ATPγS β- and γ-phosphates, respectively. Besides, the ATPγS α- and γ-phosphates both establish hydrogen bonds with the side chain of K_{181}. Additionally, two magnesium ions are coordinated to the phosphates of the nucleotide. One Mg(II) displays a well-defined octahedral coordination sphere, including the α- and β-phosphates, the side chains of the conserved N_{281} and D_{293} and two water molecules. The other Mg(II) is hexacoordinated and binds to the ATPγS γ-phosphate, the side chain of D_{293} and four water molecules (an additional water occupies the place

of the γ-phosphate in the ADP containing PknG structure). This coordination is reminiscent of that observed for human kinase Aurora A (PDB code 1MQ4 (Nowakowski et al., 2002)).

PknG binds extended peptide substrates

The absence of an arginine residue preceding the invariant catalytic aspartate in the catalytic loop (D_{276} in PknG) classifies PknG as a non-RD kinase (Johnson et al., 1996). Accordingly, and as predicted for ePKs (Huse and Kuriyan, 2002; Kornev and Taylor, 2010), the activation loop is stabilized in an open and extended conformation permissive for substrate binding in the absence of phosphorylation. Notably, in the present crystal structures, the N-terminal extended segment comprising residues 83-89 (RAPDIDP) of the single PknG molecule in the asymmetric unit gets into the active site of a crystallographic symmetry mate (Fig. 4A, left panel). This interaction resembles the mode of binding of the peptide PKI within the active site of the mouse kinase PKA (PDB code 1ATP (Zheng et al., 1993)) (Fig. 4A, right panel), suggesting that in this crystal lattice PknG residues 83-89 act as a substrate mimic or pseudosubstrate with residue D_{86} occupying the place of the GarA nucleophilic threonine T_{21}. According to this model (Fig. 4B), the side chain of E_{280} in the catalytic domain of PknG would interact with the main-chain amide of GarA residue V_{19}, the amide and the carbonyl oxygen of G_{308} would contact the carbonyl oxygen and the amide of GarA T_{22}, respectively, and the side chain of T_{309} would form a hydrogen bond with the carbonyl oxygen of GarA E_{20}. This pattern is reminiscent of the binding mode of peptide substrates to ePKs, where residues equivalent to T_{309}, located within the p+1-loop, are known to be important for the interaction at the active site (Huse and Kuriyan, 2002;

Kornev and Taylor, 2010). In fact, residue T_{309} has been previously shown to be critical for PknG kinase activity, and has been predicted to be involved in substrate binding (Tiwari et al., 2009).

The preceding findings suggested that, if the interaction between $PknG_{\Delta 73,\Delta TPR}$ molecules takes place in solution as observed in the crystal structures, a phosphorylation event should occur given a threonine residue in position 86 of the PknG protein sequence. To test this hypothesis, we mutated the $PknG_{\Delta 73,\Delta TPR}$ segment 74-90 (LGGGLVEIPRAPD$_{86}$IDPL) into GarA residues 9-25 (EKDQTSDEVTVE**T**TSVF) or EKDQTSDEVTVE**A**TSVF, and then investigated the autophosphorylation activity of these PknG variants (named respectively $PknG_{\Delta 73,\Delta TPR,E\mathbf{T}TS}$ and $PknG_{\Delta 73,\Delta TPR,E\mathbf{A}TS}$). As determined by using radiolabeled [γ^{32}P]ATP and mass spectrometry (Fig. 4C and Fig. S4A), $PknG_{\Delta 73,\Delta TPR,E\mathbf{T}TS}$ incorporated one phosphate equivalent while $PknG_{\Delta 73,\Delta TPR}$ and $PknG_{\Delta 73,\Delta TPR,E\mathbf{A}TS}$ failed to show a significant autophosphorylation activity, confirming our hypothesis. Taken together, our results provide a structural framework to explain the phosphorylation of extended peptide substrates by PknG.

The role of helix αC in PknG

The catalytic core of PknG adopts the typical two-lobed structure found in STPKs, with most functionally important and conserved residues in the active site exhibiting conformations compatible with a standard ePK active state (Scherr et al., 2007; Huse and Kuriyan, 2002; Kornev and Taylor, 2010). Nevertheless, an overlay with the structure of the prototypic active state of the cAMP-dependent protein kinase A (PKA, PDB code 1ATP (Zheng et al., 1993)) shows a clearly distinct position of PknG helix αC (Fig. 5, left panel). This helix acts as mediator of multiple regulatory mechanisms in

numerous ePKs, outstandingly *via* a conserved glutamate residue (E_{91} in PKA) that forms an invariable salt bridge with the ATP-binding lysine (K_{72} in PKA). In many cases the activation of ePKs is mediated by the formation of this salt bridge, which is usually considered a hallmark of a kinase active state (Huse and Kuriyan, 2002; Kornev and Taylor, 2010). Curiously, in all available PknG crystal structures the equivalent residues, E_{198} and K_{181}, are more than 15 Å apart. To investigate the role of PknG residue E_{198} we generated and analyzed the mutant $PknG_{E198A}$. Surprisingly, this point mutant displayed the same activity as the wild type enzyme when using GarA or the 17-mer peptide as substrates (Fig. 5, right panel). This result conclusively established that neither residue E_{198} nor, consequently, the K_{181}-E_{198} salt bridge is required for PknG activity. Therefore, the above results indicated that the available PknG crystal structures are descriptive of a productive kinase conformation in the absence of the K_{181}-E_{198} salt bridge. This would imply that the active state of PknG would be more permissive than typical ePKs regarding the actual positioning of the helix αC.

DISCUSSION

The extended knowledge about ePKs structures and regulation mechanisms has enlightened the research on the evolutionary related bacterial STPKs (Wehenkel et al., 2008). However, recent results uncover a broader view of bacterial phosphosignaling systems with particular unprecedented features (Sherman and Grundner, 2014). In this work we describe novel molecular mechanisms of regulation found for a bacterial STPK, the multidomain kinase PknG from *M. tuberculosis*. We show that the N-terminal extended region and the TPR domain are both involved in the specific phosphorylation of the physiological substrate GarA. Our observations indicate a remarkable distinction between PknG and ePKs in that much of PknG machinery seems to be dedicated to assure substrate selectivity and not to tune the specific kinase activity. We suggest that this notion might represent a more extended regulatory strategy among bacterial STPKs.

The mechanisms leading to substrate selectivity described here for PknG resemble those mediated by docking interactions in ePKs, for example among MAP and AGC kinases (Biondi and Nebreda, 2003). However, the most characterized feature in ePKs is by far the regulation of the intrinsic kinase activity and the concomitant phosphorylation of substrates that possess a rather simple recognition motif surrounding the phosphorylation site (Pinna and Ruzzene, 1996). Interestingly, we found that the peptide-binding site in PknG is very similar to that of ePKs. Among the interactions predicted between the peptide substrate and the active site of PknG (Fig. 4B) one involves the side chain of residue T_{309}, located in the p+1-loop, which has been shown to be important for kinase activity in ePKs (Huse and Kuriyan, 2002; Kornev and

Taylor, 2010) and PknG itself (Tiwari et al., 2009). In addition, all known PknG phosphorylation sites contain a non polar aminoacid two positions before the phosphorylatable threonine (Fig. S4B). This residue (V_{19} in GarA) is predicted to be stabilized by van der Waals interactions within a small pocket mainly comprising hydrophobic groups. This may explain why PknG phosphorylates specifically GarA T_{21} and not T_{22}, since the latter would require a charged side chain, GarA E_{20}, binding to the hydrophobic pocket. Also, our results do not indicate strong interactions between the peptide substrate and PknG, in agreement with the high K_M exhibited by the 17-mer substrate (Fig. S1A) and with the FHA domain of GarA being the mayor determinant of substrate selectivity (Fig. 1B).

PknG has been proposed to be active in the cytoplasm of mammalian cells (Walburger et al., 2004). It is thus tempting to speculate that the PknG machinery leading to the selective phosphorylation of the *Mtb* substrate GarA may also be relevant for the phosphorylation of mammalian substrates. Suggestively, as revealed by structure 2PZI (Scherr et al., 2007), the N-terminal segment of PknG contains a P-rich region (largely conserved in the PknG family, Fig. S3) reminiscent of that present in the C-terminal tail of kinase PKA (Fig. S5A). This region has been proposed to be functionally relevant for the AGC kinases (Kannan et al., 2007), and might be important for PknG function as well. Based on the above, we speculate that STPKs substrates could be better identified as interacting partners rather than by a consensus sequence surrounding the phosphorylation site.

All available PknG crystal structures show residue E_{198} pointing out of the active site due to a tilted and outward conformation of the helix αC in the kinase N-lobe (Fig. 5, left panel). According to the criteria normally taken into account to define a STPK

conformation as productive or not, the observed PknG conformations would then be associated to kinase "off" states given the absence of a salt bridge between E_{198} and the catalytic K_{181}. However, $PknG_{E198A}$ retained the wild type PknG activity (Fig. 5, right panel), clearly showing that neither residue E_{198} nor, consequently, the K_{181}-E_{198} salt bridge is essential for kinase activity. In the context of the overall mechanism of PknG regulation, largely dedicated to control substrate specificity, the K_{181}-E_{198} salt bridge may have evolved as a mechanism enabling a higher degree of modulation of the activity towards a physiological substrate rather than as a structural requirement for kinase activity. It is tempting to speculate that such an additional level of modulation might be mediated by tyrosine phosphorylation, recently reported for several *Mtb* proteins (including PknG) (Kusebauch et al., 2014).

PknG is a non-RD kinase (Johnson et al., 1996), and, consistently, the kinase activity is not regulated by S/T phosphorylation in the activation loop. Instead, all PknG pT sites are located within the N-terminal extension of the protein, which is crucial for recruitment of the physiological substrate GarA (O'Hare et al., 2008). Here we show that PknG activity is not modulated by S/T phosphorylation, as its N-terminal extension does not affect the intrinsic activity of the kinase domain (Fig. 1B). Also, the evidence presented indicates that the main role of the FHA domain of Gar is to facilitate the docking of the substrate through FHA-pT interactions, but not to exert an allosteric effect on the PknG catalytic domain (Fig. S1B).

Our kinetic data indicates that the TPR domain of PknG has no effect on the intrinsic activity of the kinase core (Fig. 1B and Fig. S1C). However, mutant $PknG_{\Delta TPR}$ displayed a reduced ability to phosphorylate GarA (Fig. 1B), suggesting that the TPR domain contributes to stabilize the complex PknG-GarA. We propose that this could

occur *via* the stabilization of a β-hairpin in the N-terminal segment of PknG (Fig. S5B), which is crucial for GarA recruitment. Consistently, all residues involved in the series of TPR-mediated interactions observed in structure 2PZI (Scherr et al., 2007) are strictly conserved among mycobacterial PknGs (Fig. S3), suggesting that they are functionally relevant. In previous work, the TPR domain has been found to mediate the interaction between two PknG monomers in the crystalline state (Scherr et al., 2007). However, data obtained by analytical ultracentrifugation indicated that this interaction was weak in solution, even at high protein concentrations (Fig. S1D). Thus, even though TPR domains are known to be involved in protein-protein interactions in different systems (D'Andrea and Regan, 2003), it is unclear if/how this contact may be important for PknG function, and we have failed to identify elements in support of a PknG regulatory mechanism mediated by TPR-mediated kinase dimerization.

The Rdx domain is the only region identified to directly regulate the intrinsic activity of PknG (Fig. 1B). Interestingly, this domain is present in PknG orthologs within the genus *Streptomyces* and *Mycobacterium*, including several pathogenic species (Gil et al., 2013), but is missing in *Corynebacterium* PknGs (Fig. S3). In all available PknG crystal structures the Rdx domain interacts indirectly with the G-rich-loop of the catalytic domain through residue H_{185}, which is located in the loop connecting the β_3 strand and the αC helix (Fig. 2B). This contact would also restrict the motion of the αC helix, which was systematically found in a conformation that maintains the E_{198} out of the active site. However, the Rdx domain can adopt different positions relative to the PknG active site, mediated by the interplay of distinct interdomain interactions. Thus, in the present crystal structures residues E_{125} (in the Rdx domain) and H_{223} (within the kinase N-lobe) interact with each other, while no contact is observed between the Rdx

domain and the kinase C-lobe (Fig. 2B, left panel). This open conformation allows the active site to accept a nucleotide and a peptide substrate mimic (Fig. 4A). On the other hand, replacement of the nucleotide by the small molecule inhibitor AX20017 in structure 2PZI (Scherr et al., 2007) brings the Rdx domain in contact with the kinase C-lobe, whereas residues E_{125} and H_{223} are now distant from each other (Fig. 2B, right panel). In this closed conformation, the ATP phosphates would clash with the G-rich loop, and no place is left for a peptide substrate. In line with these observations, our data clearly show that the Rdx domain downregulates the kinase activity of PknG (Fig. 1B). This domain has been proposed to modulate PknG activity by sensing the redox status of the surroundings (Scherr et al., 2007; Tiwari et al., 2009). However, some controversy remains regarding the sign of this regulation. While the deletion of the Rdx domain derepresses PknG activity (as shown in this manuscript), kinase activity is reduced (Tiwari et al., 2009) or completely abolished (Scherr et al., 2007) after perturbation (and probably disruption) of the metal center by substitution of the protein ligands. It is worth noting that the structural integrity of those PknG mutants was not opportunely assessed. In addition, a MBP-$PknG_{151-750}$ deletion mutant was analyzed and only a marginal activity was detected (Tiwari et al., 2009). The differences found between this variant and $PknG_{\Delta 137}$ can be attributed to the constructions themselves and/or to the alternative set of experimental conditions employed in kinase assays. In any case, our results clearly show that the Rdx domain of PknG is not essential for the kinase activity, in contrast to previous conclusions (Scherr et al., 2007).

In conclusion, based on the presented data we propose a model for the modulation of PknG kinase activity on its physiological substrate GarA. According to

this model, the N-terminal extension and the TPR domain of PknG work jointly in optimizing the affinity for the *Mtb* substrate GarA, whereas the Rdx domain (which may respond to the redox state of the environment) regulates the intrinsic PknG kinase activity by restricting the accessibility of the active site.

Very few representative members of the bacterial STPKs group have been crystallized and investigated in detail so far. We envisage that the regulation of the kinase activity based on substrate selectivity might be more widely distributed among bacterial STPKs. Such mechanisms may, in turn, enable the development of antibiotics with novel modes of action targeting different STPKs in *Mtb* and other pathogenic bacteria.

EXPERIMENTAL PROCEDURES

Cloning and mutagenesis

Plasmids pET28a-PknG, pET28a-PknG$_{\Delta 73}$ and pET28a-PknG$_{\Delta 73,\Delta TPR}$ were already available (O'Hare et al., 2008; Gil et al., 2013). The construction of plasmids pET28a-PknG$_{\Delta TPR}$, pET28a-PknG$_{\Delta 137}$ and pET28a-PknG$_{E198A}$ is detailed in Supplemental Experimental Procedures. Plasmids pET28a-PknG$_{\Delta 73,\Delta TPR,ETTS}$ and pET28a-PknG$_{\Delta 73,\Delta TPR,EATS}$ were constructed by GenScript using pET28a-PknG$_{\Delta 73,\Delta TPR}$ as template.

Protein production and purification

All PknG variants were over-produced in *E. coli* BL21(DE3) cells and then purified following the same protocol. Cells were harvested by centrifugation and sonicated. After clarification by centrifugation, the supernatant was loaded onto a HisTrap HP column (GE Healthcare) and the His-tagged protein was purified applying a linear imidazole gradient (20–500 mM). The PknG-containing fractions were pooled and the protein was further purified by size-exclusion chromatography on a Superdex 200 column (GE Healthcare). PknG$_{\Delta 137}$ was also prepared adding an additional purification step. Prior to the size-exclusion chromatography, the H_6 tag in PknG$_{\Delta 137}$ was removed by incubation with His_6-tagged TEV protease (van den et al., 2006), followed by separation on a Ni-NTA agarose column (Qiagen). Following the purification step by size-exclusion chromatography, fractions corresponding to the PknG peak, were pooled and concentrated, flash-frozen in liquid nitrogen and stored at -80ºC. See also Supplemental Experimental Procedures.

The substrate GarA and its FHA domain alone ($GarA_{\Delta 43}$) were prepared as previously described (England et al., 2009).

Protein kinase activity assay

Kinase activity assays were performed in 96-well plates. Each activity measurement was performed in a final volume of 20 µl, containing 50 mM Tris-HCl pH 7.4, 0.1% v/v 2-mercaptoethanol, 10 mM $MnCl_2$, 100 µM [γ^{32}P]ATP (5-50 cpm/pmol), and 330 µM 17-mer peptide or 25 µM Gar as substrate. The enzyme concentration in the assays was 0.3-1.5 µM and 0.15-0.45 µM when using the 17-mer peptide or GarA as substrates, respectively. The kinase reactions were started by the addition of 4 µl [γ^{32}P]ATP-Mn^{+2} and were performed at room temperature. The reactions were stopped by the addition of phosphoric acid and 4 µl of each reaction were spotted on P81 phosphocellulose papers (Whatman) using the epMotion 5070 (Eppendorf) workstation. The papers were washed in 0.01% phosphoric acid, dried, then measured and analyzed using the PhosphorImager (FLA-9000 Starion, Fujifilm). Each reaction was performed in duplicates (<5% variation). In all cases, specific activity values were derived from reactions performed employing three different enzyme concentrations within the indicated ranges (<10% variation), verifying a linear dependence of activity with PknG concentration. Each assay was performed at least twice. The proportion of 17-mer peptide or GarA consumed in the reactions was lower than 10% and 30%, respectively. GarA consumption was verified to be linear in time up to 50% its initial concentration. Under the experimental conditions employed to test phosphorylation of the 17-mer peptide or GarA, PknG autophosphorylation represented less than 5% of

the total signal. The measured signal was at least five times higher than the lecture on the background.

H_6 tagged $PknG_{\Delta 137}$ and untagged $PknG_{\Delta 137}$ showed the same kinetic behavior.

Crystallization and data collection

Crystallization screenings were carried out using the sitting-drop vapor diffusion method and a Mosquito nanolitre-dispensing crystallization robot (TTP Labtech). Following optimization, crystals of $PknG_{\Delta 73,\Delta TPR}$ + ADP and $PknG_{\Delta 73,\Delta TPR}$ + ATPγS grew after 10-15 days from a 20-30 mg/ml solution of protein supplemented with 2-4 mM ADP or ATPγS, respectively, by mixing 1 µl of protein solution and 1 µl of mother liquor (100 mM Hepes, 35% w/v PEG 4000, 200 mM $CaCl_2$, pH 7.5), in a hanging drop setup with 1 ml mother liquor in the reservoir, at 18ºC. Single crystals reaching a size of ~ 300 µm were cryprotected in mother liquor containing 25% glycerol and flash-frozen in liquid nitrogen. X-ray diffraction data were collected at the synchrotron beamlines Proxima 1 (Synchrotron Soleil, Saint-Aubin, France) and ID23-1 (ESRF, Grenoble, France) at 100 K. Employed wavelengths were 0.973 Å and 1.28189 Å for $PknG_{\Delta 73,\Delta TPR}$ + ADP and $PknG_{\Delta 73,\Delta TPR}$ + ATPγS crystals, respectively. The diffraction data were processed using XDS (Kabsch, 2010) and scaled with Aimless or Scala from the CCP4 program suite (Winn et al., 2011).

Structure determination and refinement

The crystal structure of $PknG_{\Delta 73,\Delta TPR}$ + ADP was solved by molecular replacement using the program Phaser (McCoy et al., 2007) and the atomic coordinates of PknG residues 74-405 from PDB 2PZI as search probe. The rubredoxin domain and some fractions of

the kinase N-lobe were removed during the firsts rounds of refinement and were subsequently rebuilt through iterative cycles of manual model building with COOT (Emsley et al., 2010) and refinement with BUSTER (Bricogne et al., 2011). The structure of $PknG_{\Delta 73,\Delta TPR}$ + ATPγS was solved using the refined coordinates of protein atoms in $PknG_{\Delta 73,\Delta TPR}$ + ADP. Ligand molecules were manually placed in *mFo–DFc* sigma-A-weighted electron density maps employing COOT, and the resulting models were refined as described above. The final models were validated through the Molprobity server (http://molprobity.biochem.duke.edu) (Chen et al., 2010). The two crystal structures are very similar to each other, with an RMSD of 0.13 Å for 321 alpha carbons. In each case, the final model contained 98% of residues within favored regions of Ramachandran plot, with no outliers. Figures were generated and rendered with Pymol 1.5.0.2. (Schrödinger, LLC). Atomic coordinates and structure factors have been deposited in the Protein Data Bank under the accession codes 4Y0X ($PknG_{\Delta 73,\Delta TPR}$ + ADP) and 4Y12 ($PknG_{\Delta 73,\Delta TPR}$ + ATPγS).

AUTHOR CONTRIBUTIONS

MNL designed experiments, prepared proteins, carried out crystallographic studies and structural analysis, performed kinase activity assays, analyzed data and wrote the paper; MG prepared constructs pET28a-PknG$_{\Delta TPR}$ and pET28a-PknG$_{\Delta 137}$ and carried out mass spectrometry analyses; GAL performed molecular modeling; NB prepared plasmid pET28a-PknG$_{E198A}$ and performed analytical ultracentrifugation experiments; RD designed and performed mass spectrometry studies; RMB designed kinase activity assays, analyzed data and wrote the paper; PMA designed research, analyzed data and wrote the paper.

ACKNOWLEDGEMENTS

We thank Ariel Mechaly and Marco Bellinzoni for insightful discussions, Ahmed Haouz and Patrick Weber for their help with robot-driven crystallization screenings, and Bertrand Raynal and Sylviane Hoos for their help with analytical ultracentrifugation experiments. MNL received fellowships from the EMBO (European Molecular Biology Organization) and the Fondation pour la Recherche Médicale (FRM, France). This work was supported by grants from the Institut Pasteur, the CNRS (France), the Agence Nationale de la Recherche (ANR, France, contract number ANR-09-BLAN-0400) and the European Commission Seventh Framework Programme (contract HEALTH-F3-2011-260872). RMB acknowledges support from DFG (grant BI 1044/12-1).

REFERENCE LIST

Av-Gay,Y. and Everett,M. (2000). The eukaryotic-like Ser/Thr protein kinases of Mycobacterium tuberculosis. Trends Microbiol. *8*, 238-244.

Barthe,P., Roumestand,C., Canova,M.J., Kremer,L., Hurard,C., Molle,V., and Cohen-Gonsaud,M. (2009). Dynamic and structural characterization of a bacterial FHA protein reveals a new autoinhibition mechanism. Structure. *17*, 568-578.

Biondi,R.M. and Nebreda,A.R. (2003). Signalling specificity of Ser/Thr protein kinases through docking-site-mediated interactions. Biochem. J. *372*, 1-13.

Bricogne,G. et al (2011). BUSTER version 2.11.4. Cambridge, United Kingdom: Global Phasing Ltd.

Chao,J., Wong,D., Zheng,X., Poirier,V., Bach,H., Hmama,Z., and Av-Gay,Y. (2010). Protein kinase and phosphatase signaling in Mycobacterium tuberculosis physiology and pathogenesis. Biochim. Biophys. Acta *1804*, 620-627.

Chen,V.B., Arendall,W.B., III, Headd,J.J., Keedy,D.A., Immormino,R.M., Kapral,G.J., Murray,L.W., Richardson,J.S., and Richardson,D.C. (2010). MolProbity: all-atom structure validation for macromolecular crystallography. Acta Crystallogr. D Biol. Crystallogr. *66*, 12-21.

Cole,S.T. et al (1998). Deciphering the biology of Mycobacterium tuberculosis from the complete genome sequence. Nature *393*, 537-544.

Cowley,S. et al (2004). The Mycobacterium tuberculosis protein serine/threonine kinase PknG is linked to cellular glutamate/glutamine levels and is important for growth in vivo. Mol. Microbiol. *52*, 1691-1702.

D'Andrea,L.D. and Regan,L. (2003). TPR proteins: the versatile helix. Trends Biochem. Sci. *28*, 655-662.

Duran,R., Villarino,A., Bellinzoni,M., Wehenkel,A., Fernandez,P., Boitel,B., Cole,S.T., Alzari,P.M., and Cervenansky,C. (2005). Conserved autophosphorylation pattern in activation loops and juxtamembrane regions of Mycobacterium tuberculosis Ser/Thr protein kinases. Biochem. Biophys. Res. Commun. *333*, 858-867.

Emsley,P., Lohkamp,B., Scott,W.G., and Cowtan,K. (2010). Features and development of Coot. Acta Crystallographica Section D *66*, 486-501.

England,P., Wehenkel,A., Martins,S., Hoos,S., Andre-Leroux,G., Villarino,A., and Alzari,P.M. (2009). The FHA-containing protein GarA acts as a phosphorylation-dependent molecular switch in mycobacterial signaling. FEBS Lett. *583*, 301-307.

Gil,M., Grana,M., Schopfer,F.J., Wagner,T., Denicola,A., Freeman,B.A., Alzari,P.M., Batthyany,C., and Duran,R. (2013). Inhibition of Mycobacterium tuberculosis PknG by

non-catalytic rubredoxin domain specific modification: reaction of an electrophilic nitro-fatty acid with the Fe-S center. Free Radic. Biol. Med. *65*, 150-161.

Huse,M. and Kuriyan,J. (2002). The conformational plasticity of protein kinases. Cell *109*, 275-282.

Johnson,L.N., Noble,M.E., and Owen,D.J. (1996). Active and inactive protein kinases: structural basis for regulation. Cell *85*, 149-158.

Kabsch,W. (2010). XDS. Acta Crystallogr. D. Biol. Crystallogr. *66*, 125-132.

Kannan,N., Haste,N., Taylor,S.S., and Neuwald,A.F. (2007). The hallmark of AGC kinase functional divergence is its C-terminal tail, a cis-acting regulatory module. Proc. Natl. Acad. Sci. U. S. A *104*, 1272-1277.

Kornev,A.P. and Taylor,S.S. (2010). Defining the conserved internal architecture of a protein kinase. Biochim. Biophys. Acta *1804*, 440-444.

Kusebauch,U., Ortega,C., Ollodart,A., Rogers,R.S., Sherman,D.R., Moritz,R.L., and Grundner,C. (2014). Mycobacterium tuberculosis supports protein tyrosine phosphorylation. Proc. Natl. Acad. Sci. U. S. A *111*, 9265-9270.

McCoy,A.J., Grosse-Kunstleve,R.W., Adams,P.D., Winn,M.D., Storoni,L.C., and Read,R.J. (2007). Phaser crystallographic software. J. Appl. Crystallogr. *40*, 658-674.

Niebisch,A., Kabus,A., Schultz,C., Weil,B., and Bott,M. (2006). Corynebacterial protein kinase G controls 2-oxoglutarate dehydrogenase activity via the phosphorylation status of the OdhI protein. J. Biol. Chem. *281*, 12300-12307.

Nott,T.J. et al (2009). An intramolecular switch regulates phosphoindependent FHA domain interactions in Mycobacterium tuberculosis. Sci. Signal. *2*, ra12.

Nowakowski,J. et al (2002). Structures of the cancer-related Aurora-A, FAK, and EphA2 protein kinases from nanovolume crystallography. Structure. *10*, 1659-1667.

O'Hare,H.M. et al (2008). Regulation of glutamate metabolism by protein kinases in mycobacteria. Mol. Microbiol. *70*, 1408-1423.

Pinna,L.A. and Ruzzene,M. (1996). How do protein kinases recognize their substrates? Biochim. Biophys. Acta *1314*, 191-225.

Prisic,S., Dankwa,S., Schwartz,D., Chou,M.F., Locasale,J.W., Kang,C.M., Bemis,G., Church,G.M., Steen,H., and Husson,R.N. (2010). Extensive phosphorylation with overlapping specificity by Mycobacterium tuberculosis serine/threonine protein kinases. Proc. Natl. Acad. Sci. U. S. A *107*, 7521-7526.

Sassetti,C.M., Boyd,D.H., and Rubin,E.J. (2003). Genes required for mycobacterial growth defined by high density mutagenesis. Mol. Microbiol. *48*, 77-84.

Scherr,N., Honnappa,S., Kunz,G., Mueller,P., Jayachandran,R., Winkler,F., Pieters,J., and Steinmetz,M.O. (2007). Structural basis for the specific inhibition of protein kinase G, a virulence factor of Mycobacterium tuberculosis. Proc. Natl. Acad. Sci. U. S. A *104*, 12151-12156.

Scherr,N., Muller,P., Perisa,D., Combaluzier,B., Jeno,P., and Pieters,J. (2009). Survival of pathogenic mycobacteria in macrophages is mediated through autophosphorylation of protein kinase G. J. Bacteriol. *191*, 4546-4554.

Sherman,D.R. and Grundner,C. (2014). Agents of change - concepts in Mycobacterium tuberculosis Ser/Thr/Tyr phosphosignalling. Mol. Microbiol. *94*, 231-241.

Tiwari,D., Singh,R.K., Goswami,K., Verma,S.K., Prakash,B., and Nandicoori,V.K. (2009). Key residues in Mycobacterium tuberculosis protein kinase G play a role in regulating kinase activity and survival in the host. J. Biol. Chem. *284*, 27467-27479.

Traxler,P. and Furet,P. (1999). Strategies toward the design of novel and selective protein tyrosine kinase inhibitors. Pharmacol. Ther. *82*, 195-206.

van den,B.S., Lofdahl,P.A., Hard,T., and Berglund,H. (2006). Improved solubility of TEV protease by directed evolution. J. Biotechnol. *121*, 291-298.

Ventura,M., Rieck,B., Boldrin,F., Degiacomi,G., Bellinzoni,M., Barilone,N., Alzaidi,F., Alzari,P.M., Manganelli,R., and O'Hare,H.M. (2013). GarA is an essential regulator of metabolism in Mycobacterium tuberculosis. Mol. Microbiol. *90*, 356-366.

Walburger,A., Koul,A., Ferrari,G., Nguyen,L., Prescianotto-Baschong,C., Huygen,K., Klebl,B., Thompson,C., Bacher,G., and Pieters,J. (2004). Protein kinase G from pathogenic mycobacteria promotes survival within macrophages. Science *304*, 1800-1804.

Wehenkel,A. et al (2008). Mycobacterial Ser/Thr protein kinases and phosphatases: physiological roles and therapeutic potential. Biochim. Biophys. Acta *1784*, 193-202.

Winn,M.D. et al (2011). Overview of the CCP4 suite and current developments. Acta Crystallographica Section D *67*, 235-242.

Zheng,J., Trafny,E.A., Knighton,D.R., Xuong,N.H., Taylor,S.S., Ten Eyck,L.F., and Sowadski,J.M. (1993). 2.2 A refined crystal structure of the catalytic subunit of cAMP-dependent protein kinase complexed with MnATP and a peptide inhibitor. Acta Crystallogr. D Biol. Crystallogr. *49*, 362-365.

FIGURE LEGENDS

Figure 1. *PknG deletion mutants and their relative kinase activities.* (A) The left panel shows a schema representing the different PknG constructions (wild type and deletion mutants) used in this study. The cluster of autophosphorylation sites in the N-terminal region of PknG is indicated by a (P) symbol. The right panel shows a Coomassie-stained SDS-PAGE of the purified PknG constructions; lines 1 to 4 correspond to H_6-tagged wild type PknG, $PknG_{\Delta 73}$, $PknG_{\Delta TPR}$ and $PknG_{\Delta 73,\Delta TPR}$, respectively; line 5 corresponds to TEV-treated $PknG_{\Delta 137}$. (B) Relative kinase activity of PknG variants against the physiological substrate GarA (left panel) and the GarA derived 17-mer peptide $SDEVTVET_{21}TSVFRADFL$ (right panel). Measurements were performed at least twice; error bars represent the scattering of measured values. See also Figures S1, S3 and S5.

Figure 2. *The structure of PknG suggests a regulatory role for the Rdx domain by opening/closing the active site entrance.* (A) Left: Overall structure of $PknG_{\Delta 73\Delta TPR}$ (this work) with the Rdx domain (in pink) bound to the N-terminal lobe of the catalytic domain (in yellow). At the bottom of the open substrate-binding cleft, the ATPγS molecule is shown in stick representation. Center: Comparison of the $PknG_{\Delta 73\Delta TPR}$ structure (pink and yellow ribbons) with the structure of PknG bound to inhibitor AX20017 (PDB code 2PZI (Scherr et al., 2007), shown in grey), illustrating the movement of the Rdx domain. Right: Molecular surface representation of 2PZI (in grey) with a closed substrate-binding cleft. In each case, the metal ion within the Rdx domain is shown as a sphere. (B) Interactions between the Rdx domain and the kinase core of PknG. Left: The structure of $PknG_{\Delta 73\Delta TPR}$ is shown in pink (Rdx domain), gray (N-

terminal tail), green (β_3 strand, αC helix, and the loop conecting these motifs), cyan (β_4 and β_5 strands and the loop between them) and yellow (the remaining of the kinase N-lobe). Right: Structure 2PZI is shown in gray. In sticks, N, O, P and S atoms are colored in blue, red, orange and dark yellow, respectively. Dashed lines represent atomic interactions. See also Figures S2 and S3.

Figure 3. *The ATP binding site of PknG.* The protein is depicted as yellow ribbons. The ATPγS molecule and the protein residues interacting with it are shown in sticks with atoms colored by type (C, yellow; N, blue; O, red; P, orange; S, dark yellow). Water molecules are presented as red spheres or stars and magnesium atoms are shown as green spheres. The *2mFo–DFc* electron density is contoured to 1.5 σ and represented as a blue mesh. Dashed lines represent atomic interactions.

Figure 4. *A peptide substrate mimic within the active site of PknG.* (A) A portion of the N-terminal segment (residues shown in sticks) of a PknG molecule in the crystal gets into the active site of a symmetry related molecule. The right panel shows a zoom into PknG active site. The conformation of the PknG peptide substrate mimic resembles that of peptide PKI (in sticks with green C atoms) within the active site of mouse PKA (PDB code 1ATP). Residue D_{86} occupies the position of the phosphorylatable T_{21} in GarA. (B) Model of peptide $TVET_{21}TSV$, corresponding to GarA residues 18-24, within the substrate-binding site of PknG. The protein is shown as yellow ribbons, except for the p+1 loop which is depicted in cyan, and the peptide as a violet ribbon. Residues $VET_{21}T$ in the peptide substrate, PknG residues E_{280}, G_{308} and T_{309} and the nucleotide are shown in sticks and atoms are colored by type: C, violet in the peptide substrate,

cyan in PknG T_{309} and yellow in PknG G_{308}, PknG E_{280} and the nucleotide; N, blue; O, red; P, orange; S, dark yellow. Magnesium atoms are shown as green spheres. Dashed lines represent atomic interactions. The total potential energy of complex $PknG_{\Delta 73,\Delta TPR}$/TVETTSV was -10,255 kcal/mol and the interaction energy was -54 kcal/mol, similar to the values found for complex $PknG_{\Delta 73,\Delta TPR}$/RAPDIDP (-10,374 and -68, respectively). (c) Autophosphorylation activity of PknG mutants. Measurements were performed employing 30 µM of enzyme in all cases. See also Figure S4.

Figure 5. *Functionally important and conserved residues within the active site of PknG.* Left: Comparison of $PknG_{\Delta 73,\Delta TPR}$ active site with that of PKA (PDB code 1ATP) in its active "on" state. $PknG_{\Delta 73,\Delta TPR}$ is shown as gray ribbons, except for the highlighted motifs, and sticks with C atoms colored as the label of the corresponding motif or residue. PKA is presented as green ribbons and sticks with green C atoms. The ATPγS molecule bound to the $PknG_{\Delta 73,\Delta TPR}$ active site is shown in sticks with gray C atoms and magnesium ions are depicted as green spheres. The other atoms in sticks are colored by type: N, blue; O, red; P, orange; S, dark yellow. The dashed line represents the salt bridge between PKA residues K_{72} and E_{91}. PKA residue numbers are shown between brackets. Right: Relative kinase activity of wild type PknG and $PknG_{E198A}$ against GarA and the GarA derived 17-mer peptide SDEVTVET$_{21}$TSVFRADFL. Measurements were performed at least twice; error bars represent the scattering of measured values. See also Figure S3.

TABLES

Table 1. *Data collection and refinement statistics*.

	$PknG_{\Delta 73,\Delta TPR}$ + ADP (PDB code: 4Y0X)	$PknG_{\Delta 73,\Delta TPR}$ + ATPγS (PDB code: 4Y12)
Data collection		
Space group	C121	C121
Cell dimensions		
a, *b*, *c* (Å)	75.92, 37.25, 108.52	75.45, 37.18, 108.03
α, β, γ (°)	90.00, 97.74, 90.00	90.00, 97.93, 90.00
Resolution (Å)	37.61-1.74 (1.77-1.74) [a]	37.37-1.90 (2.00-1.90)
R_{sym} or R_{merge}	0.067 (0.794)	0.073 (0.774)
$I / \sigma I$	18.4 (2.1)	12.8 (2.6)
Completeness (%)	99.9 (99.9)	98 (96.4)
Redundancy	5.0 (3.7)	7.4 (7.2)
Refinement		
Resolution (Å)	37.61-1.74 (1.77-1.74)	37.37-1.90 (2.00-1.90)
No. reflections	31,242	23,246
R_{work} / R_{free}	19.72/20.87	19.56/21.16
No. atoms		
Protein	2,429	2,379
Ligand/Mg(II)/Zn(II)	27(ADP)/2/1	31(ATPγS)/2/1
Water	229	171
B-factors		
Protein	38.17	44.61
Ligand/ion	28.80	40.50
Water	44.88	47.78
R.m.s. deviations		
Bond lengths (Å)	0.01	0.01
Bond angles (°)	1.02	1.05

*One protein crystal was employed for structure determination in each case. Values in parentheses are for highest-resolution shell.

Figure_1
Click here to download Figure: Figure_1.tif

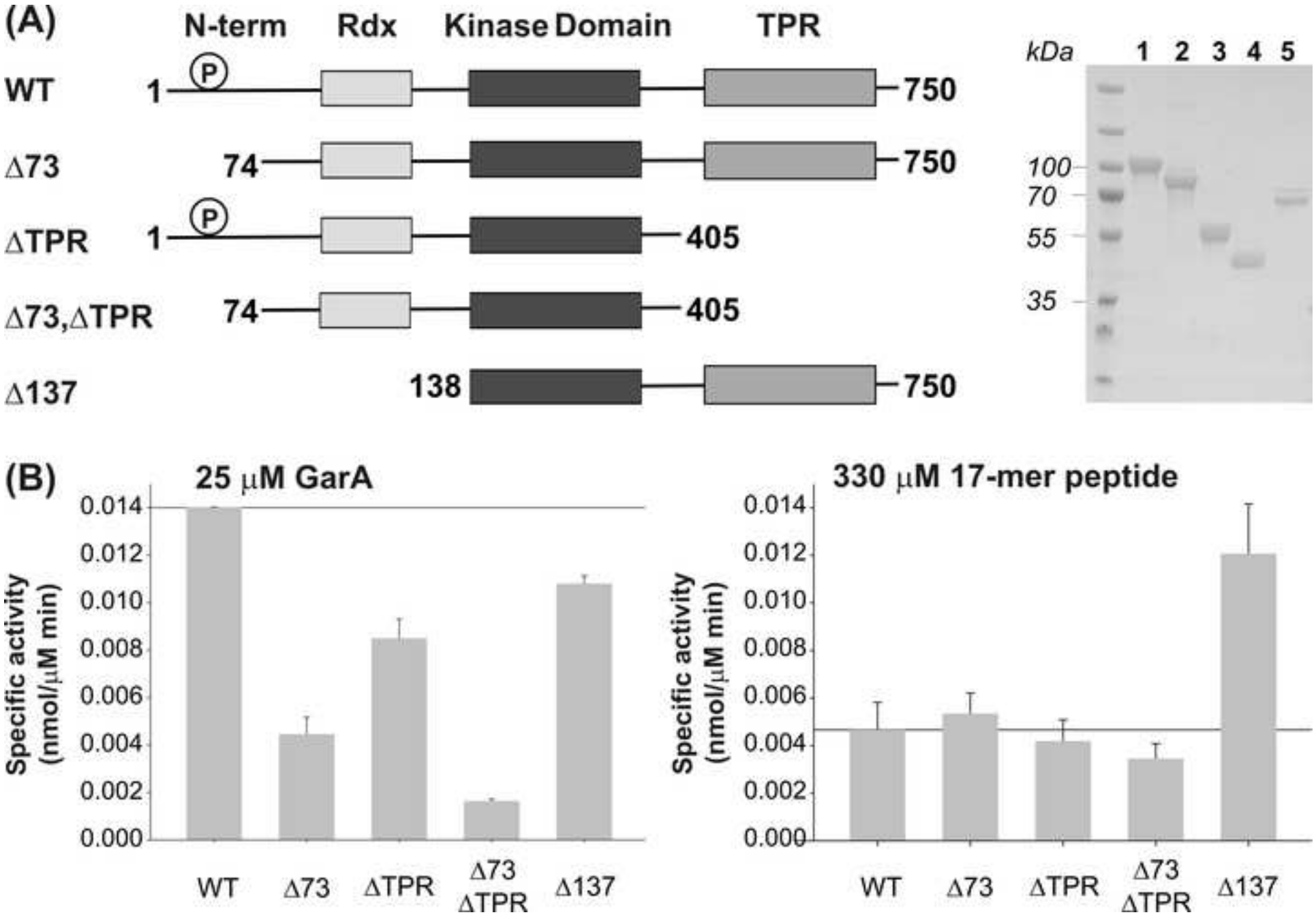

Figure_2
Click here to download Figure: Figure_2.tif

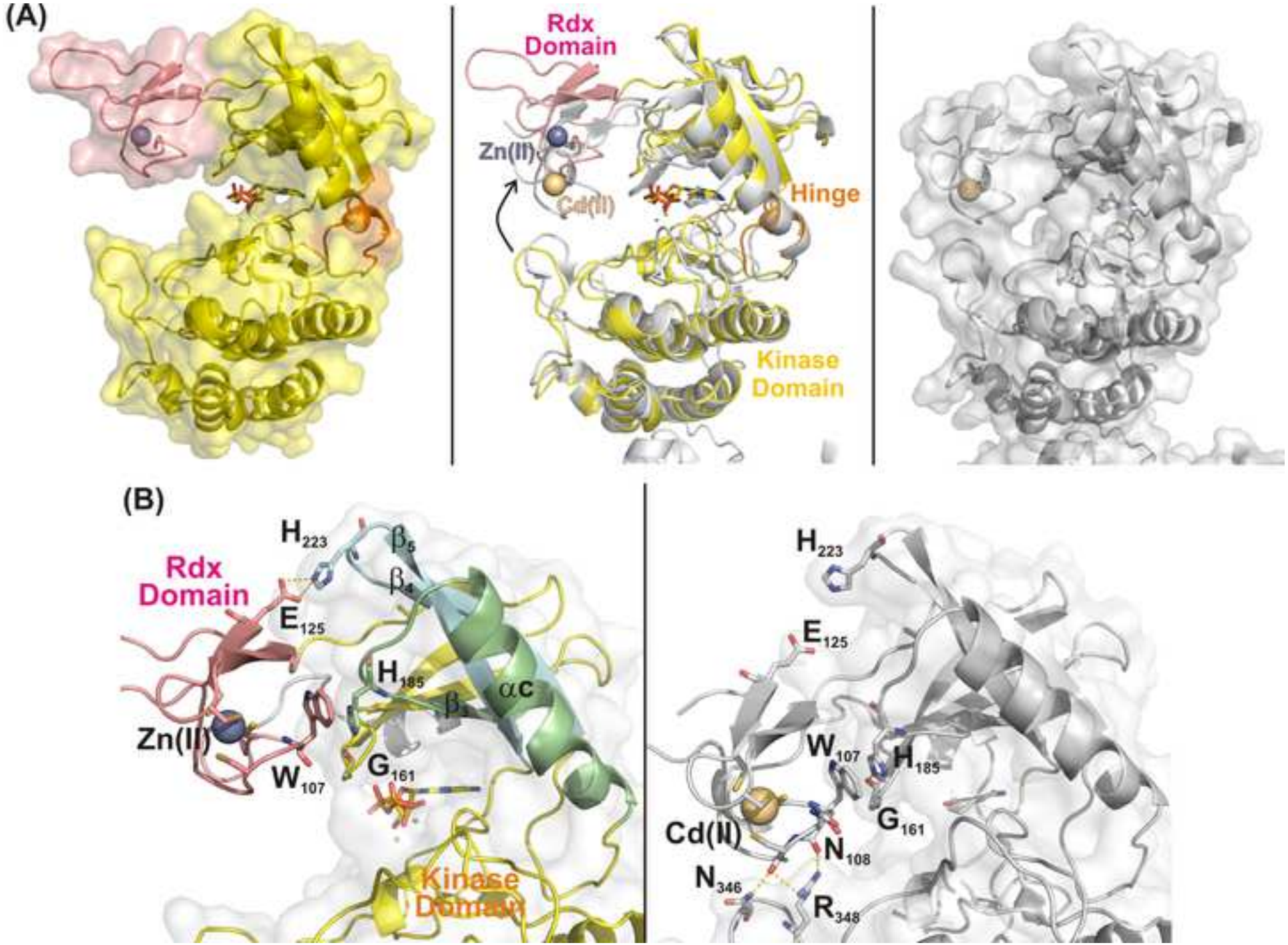

Figure_3
Click here to download Figure: Figure_3.tif

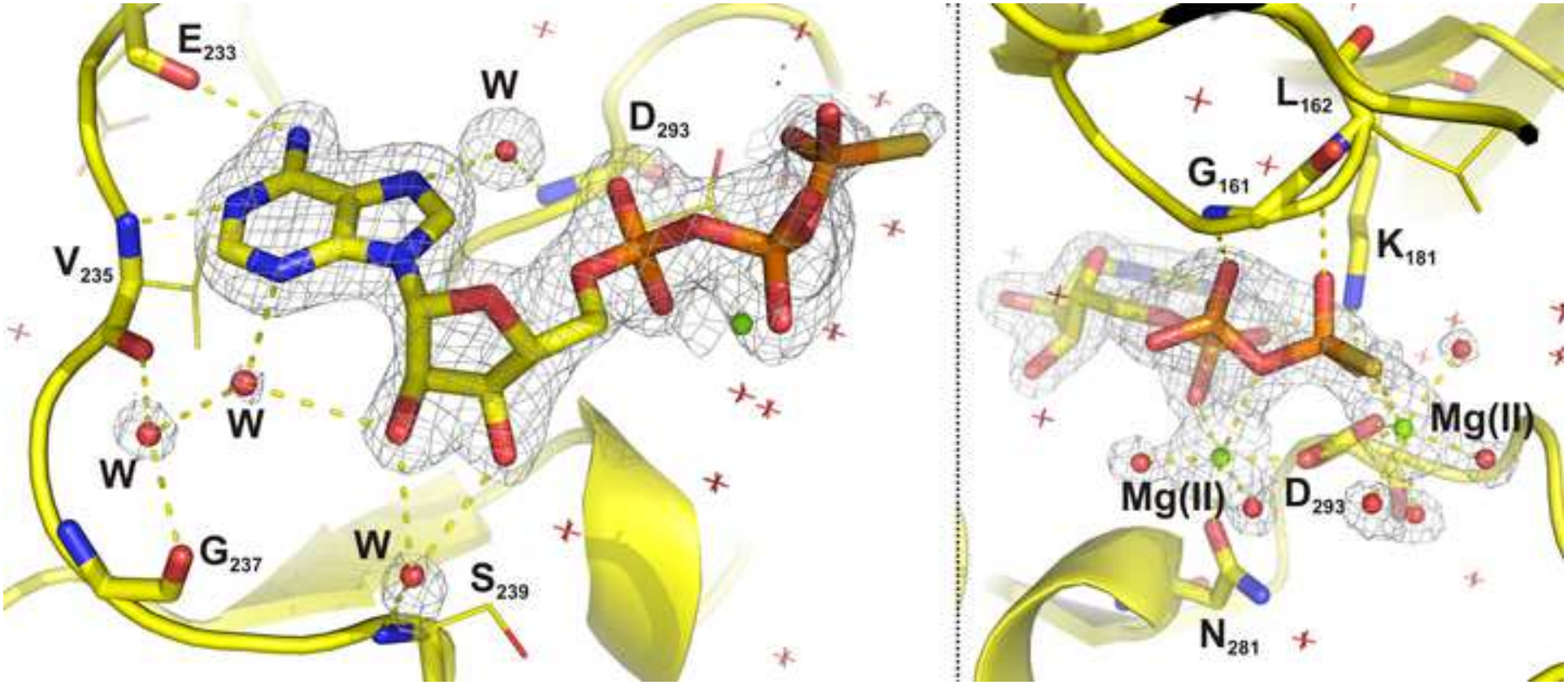

Figure_4
Click here to download Figure: Figure_4.tif

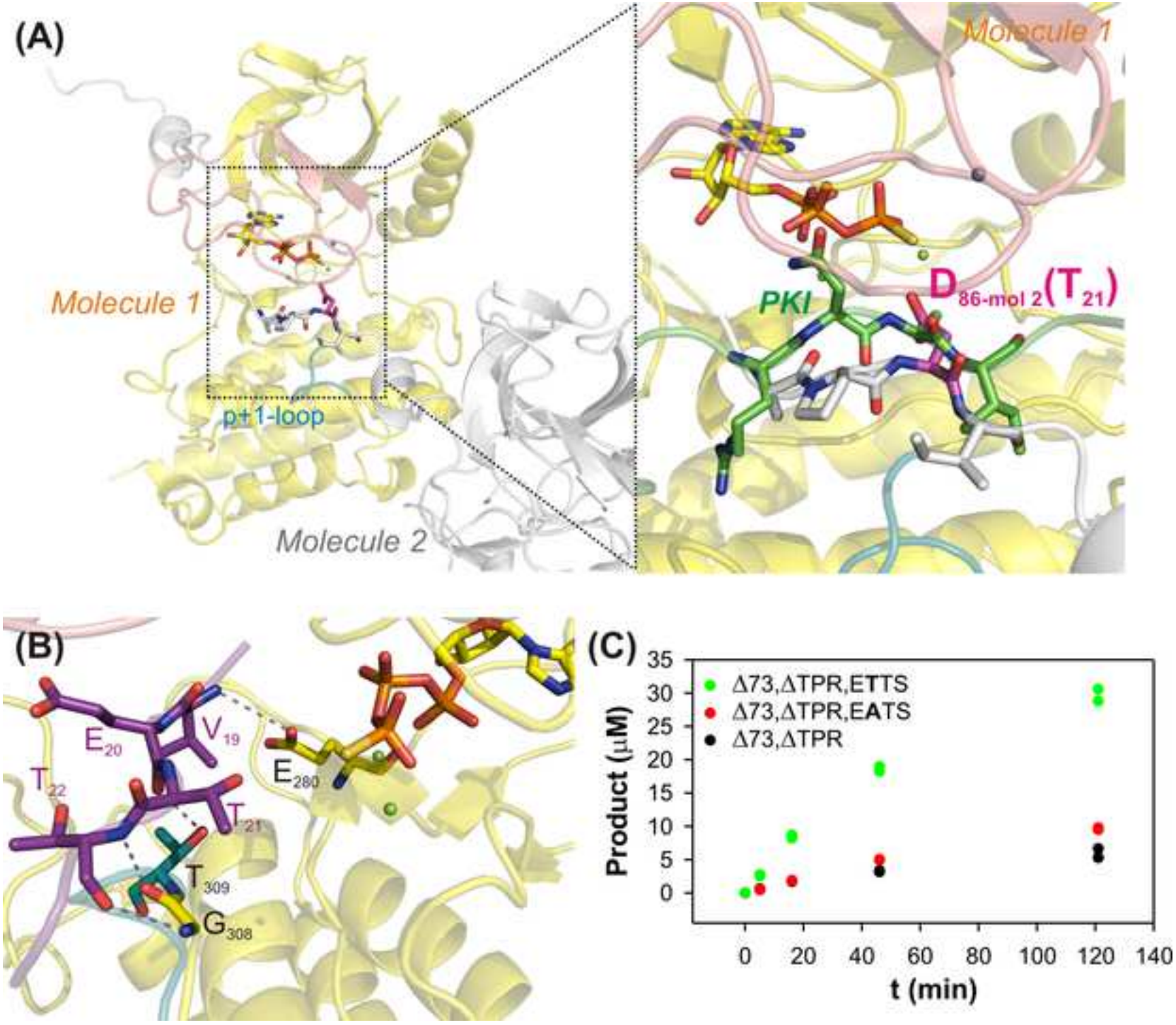

Figure_5
Click here to download Figure: Figure_5.tif

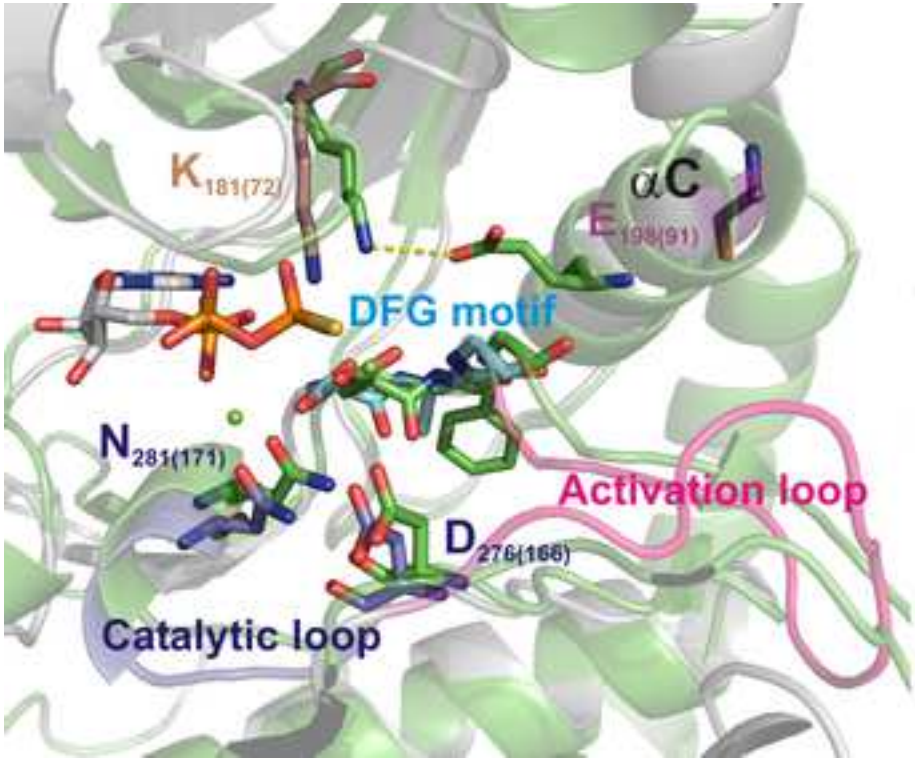

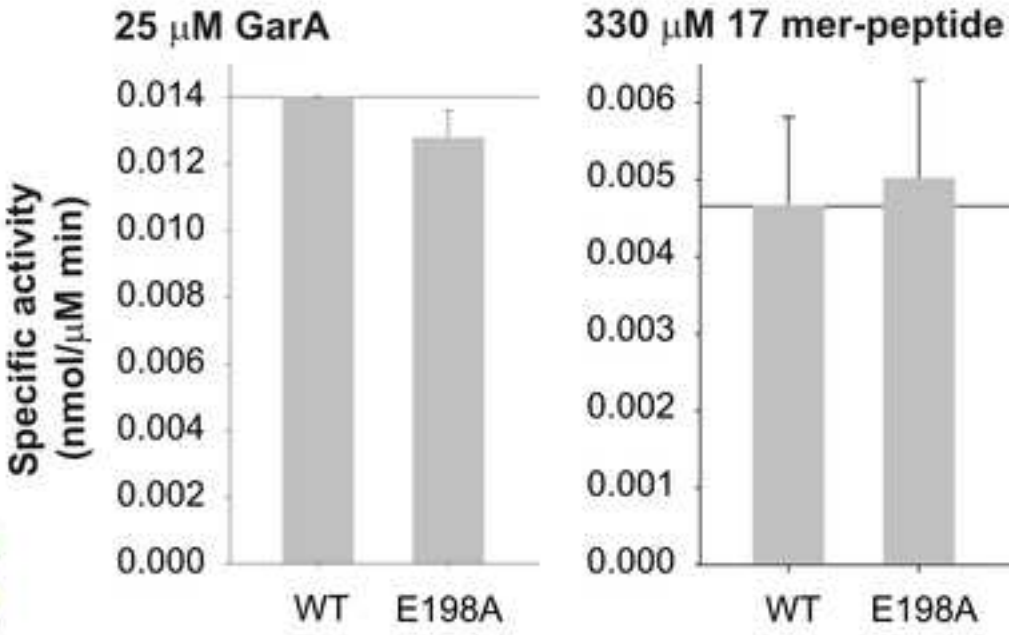

SUPPLEMENTAL INFORMATION

SUPPLEMENTAL DATA

Figure S1, related to Figure 1. *PknG domains flanking the catalytic core contribute to the selective phosphorylation of GarA*. (A) A high K_M and a low k_{cat}/K_M for the phosphorylation of the GarA derived 17-mer peptide substrate (SDEVTVET$_{21}$TSVFRADFL) by wild type PknG. The kinase activity of full-length PknG (0.8 µM) varied linearly with the concentration of the 17-mer peptide up to 1 mM (K_M > 1 mM) and the slope of the curve (k_{cat}/K_M) provides a measure of the catalytic efficiency for this substrate ((1.9 $\pm$ 0.1) 10^{-5} nmol/µM^2.min). (B) The FHA domain of GarA does not affect the phosphorylation of the 17-mer peptide substrate by wild type PknG. Substrate concentration was 1 mM. (C) The TPR domain of PknG has no effect on autophosphorylation. Protein concentration was 30 µM for the wild type enzyme and the deletion mutant. (D) Full-length PknG behaves mainly as a monomer (70%) at 1 mg/ml. Analytical ultracentrifugation, result of analysis by sedimentation velocity.

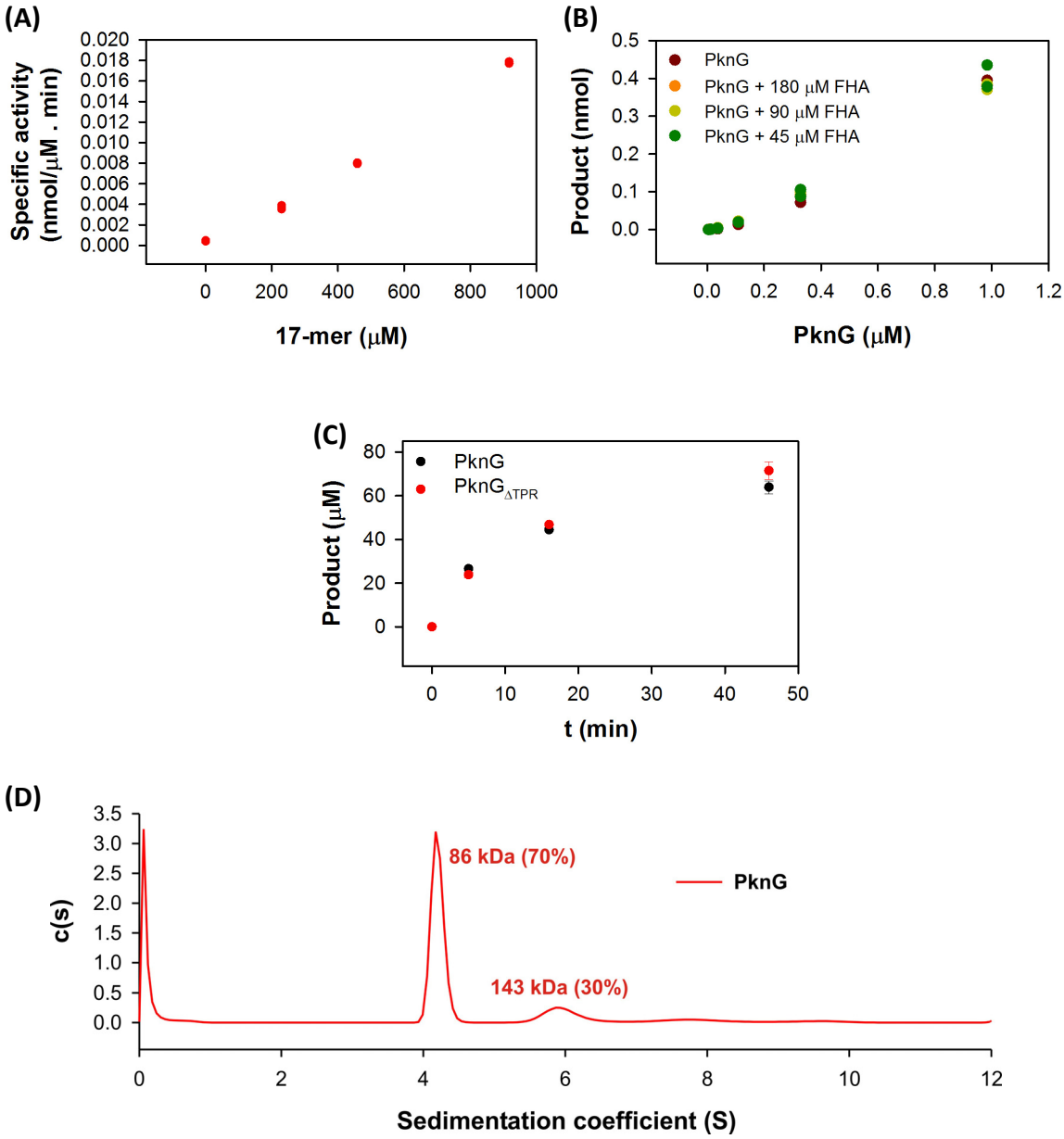
(A)
Specific activity (nmol/μM . min)
0.020
0.018
0.016
0.014
0.012
0.010
0.008
0.006
0.004
0.002
0.000
0
200
400
600
800
1000
17-mer (μM)
(B)
Product (nmol)
0.5
0.4
0.3
0.2
0.1
0.0
PknG
PknG + 180 μM FHA
PknG + 90 μM FHA
PknG + 45 μM FHA
0.0
0.2
0.4
0.6
0.8
1.0
1.2
PknG (μM)
(C)
Product (μM)
80
60
40
20
0
PknG
PknG$_{\Delta TPR}$
0
10
20
30
40
50
t (min)
(D)
c(s)
3.5
3.0
2.5
2.0
1.5
1.0
0.5
0.0
86 kDa (70%)
PknG
143 kDa (30%)
0
2
4
6
8
10
12
Sedimentation coefficient (S)

Figure S2, related to Figure 2. *The Rdx domain of PknG.* (A) A fluorescence emission spectrum obtained from a $PknG_{\Delta 73,\Delta TPR}$ crystal pointed out the presence of significant amounts of zinc. Indeed, the analysis of X-ray anomalous diffraction data just above and bellow the Zn K edge confirmed the presence of a Zn(II) metal ligand in the Rdx domain of PknG. It is shown in pink ribbons and sticks colored by atom type (C, pink; N, blue; O, red; S, dark yellow). The Zn(II) metal ligand is shown as a grey sphere. The *2mFo–DFc* electron density is contoured to 2 σ and represented as a blue mesh. A double difference anomalous map calculated with diffraction data above (9672 eV) and below (9640 eV) the Zn K-edge is shown in cyan and contoured at 4 σ. Dashed lines represent atomic interactions. PDB code 4Y12. (B) Rdx domains normally bind iron as metal cofactor (Sieker et al., 1994). In effect, an UV-vis electronic spectrum of $PknG_{\Delta 73,\Delta TPR}$ in solution revealed an absorption band centered at 490 nm, consistent with a Cys-Fe(III) ligand to metal charge transfer band (Bonomi et al., 1998). On the other hand, the low molar extinction coefficient observed (~ 500 M^{-1} cm^{-1}) indicated that only a small fraction of the protein sample (5-10%) contained iron as ligand. All PknG variants containing the Rdx domain presented similar results. It has been shown that in some rubredoxin containing proteins iron and zinc exchange as an artifact of protein overproduction in *E. coli* cells, without substantially affecting the coordination geometry in the metal binding site (Bonomi et al., 1998).

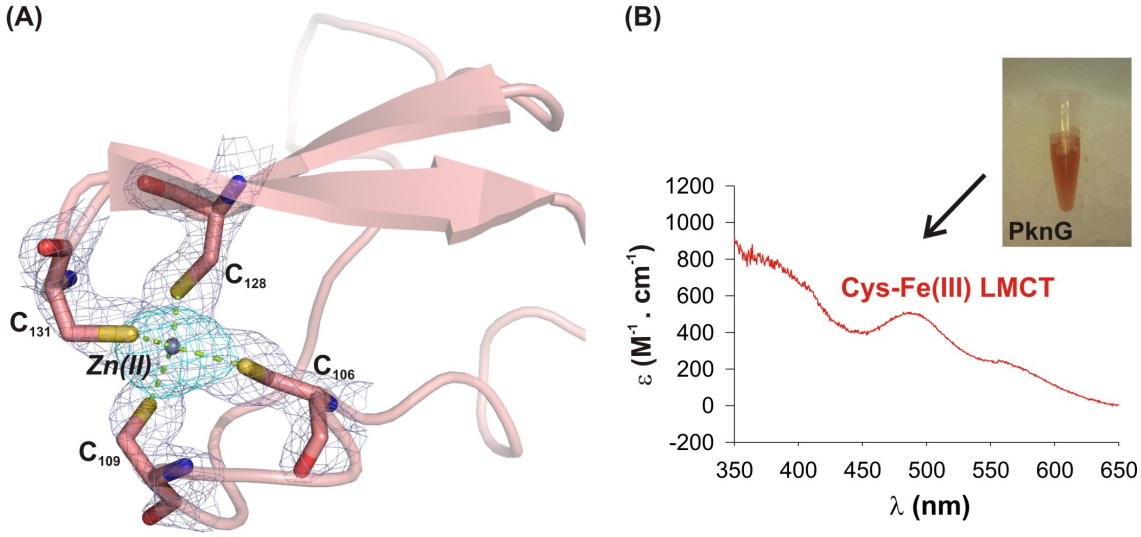

Figure S3, related to Figures 1, 2 and 5 and section Discussion. *Multiple sequence alignment of PknG homologs.* Residues of PknG from *M. tuberculosis* involved in interactions (as described in the main text) between the Rdx domain and the kinase core are signaled in red. Similarly, residues involved in interactions between the TPR domain, the kinase core, and the N-terminal segment are signaled in green. Some motifs and secondary structure elements are indicated.

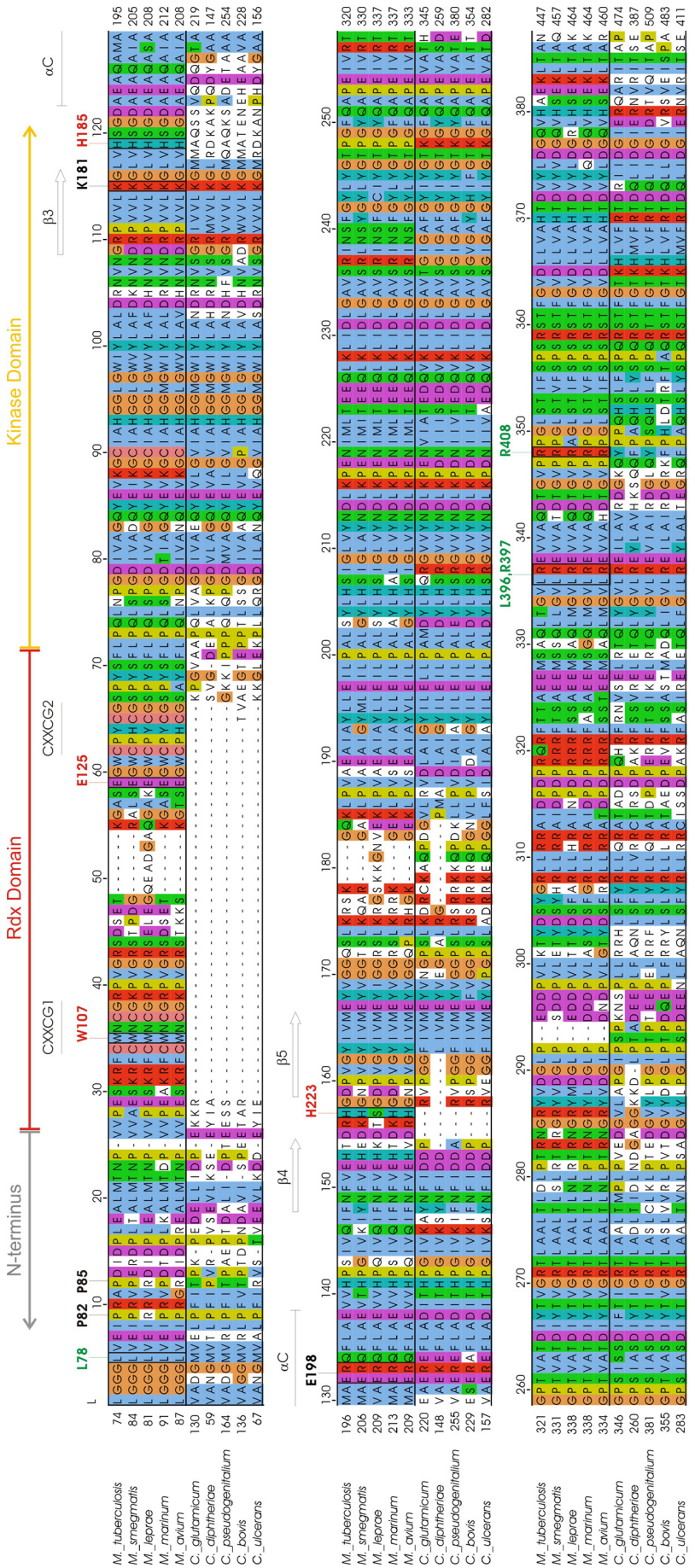

Figure S4, related to Figure 4. *The peptide binding site of PknG.* (A) Identification of $PknG_{\Delta 73,\Delta TPR,ETTS}$ phosphorylation site. MS/MS spectrum of doubly charged ion at *m*/*z* 596.70 (MH^+ 1192.4) from an endoproteinase GluC digestion of $PknG_{\Delta 73,\Delta TPR,ETTS}$ previously incubated with ATP and $MnCl_2$. The N-terminal (*b*, red-labeled) and C-terminal (*y*, blue-labeled) fragment ions that allowed the sequence 52-61 assignment and that includes a phosphorylated threonine residue (T56) are shown. Ion fragments showing neutral losses ($-H_2O$ and $-H_3PO_4$) are also indicated. *Inset*, amino acid sequence of peptide VTVEpTTSVFE, indicating major *b* and *y* ions detected by full scan MS/MS. (B) GarA residue V_{19} is predicted to be stabilized by van der Waals interactions within a small hydrophobic pocket in PknG active site. Left: model of peptide TVE**T**TSV, corresponding to GarA residues 18-24, within the active site of PknG. The peptide substrate is shown as a ribbon and sticks (residues VE**T**T) with violet C carbons. The surface of the protein is depicted with C carbons colored in yellow in the kinase core and in pink in the Rdx domain. The nucleotide within the active site is shown in sticks with yellow carbons and magnesium ions are depicted as small green spheres. N, O, P and S atoms are colored in blue, red, orange and dark yellow, respectively. Right: peptides known to be phosphorylated by PknG. They contain a non polar aminoacid two positions before the phosphorylatable threonine (in red).

(A)

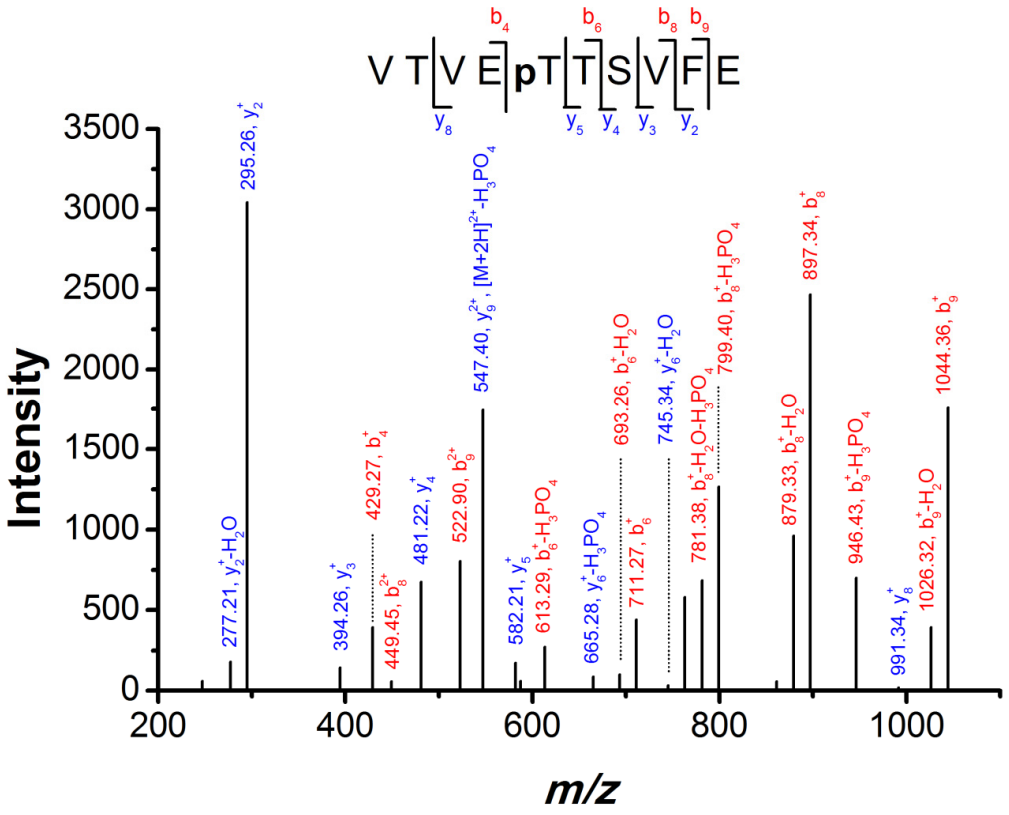
V T V E pT T S V F E
b4 b6 b8 b9
y8 y5 y4 y3 y2
Intensity
m/z
0
500
1000
1500
2000
2500
3000
3500
200
400
600
800
1000
277.21, y2+-H2O
295.26, y2+
394.26, y3+
429.27, b4+
449.45, b82+
481.22, y4+
522.90, b92+
547.40, y92+, [M+2H]2+-H3PO4
582.21, y5+
613.29, b6+-H3PO4
665.28, y6+-H3PO4
693.26, b6+-H2O
711.27, b6+
745.34, y6+-H2O
781.38, b8+-H2O-H3PO4
799.40, b8+-H3PO4
879.33, b8+-H2O
897.34, b8+
946.43, b9+-H3PO4
991.34, y8+
1026.32, b9+-H2O
1044.36, b9+

(B)

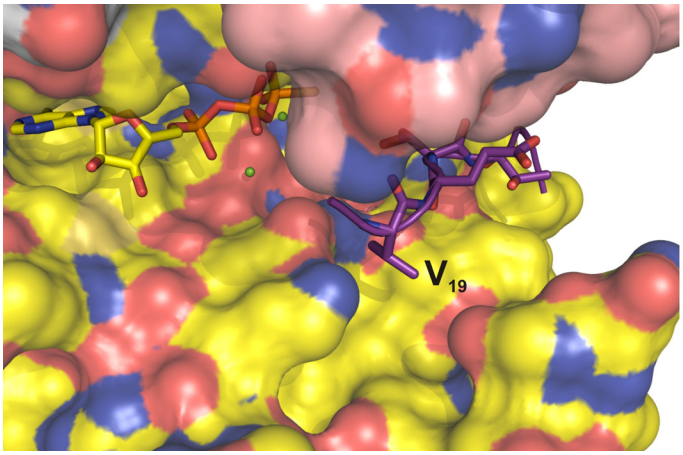
V19

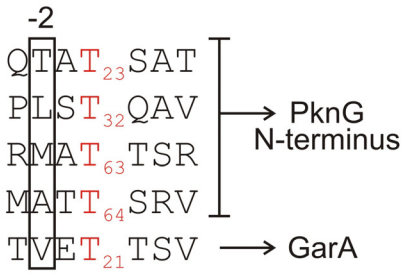
-2
QTAT23SAT
PLST32QAV
RMAT63TSR
MATT64SRV
TVET21TSV
PknG
N-terminus
GarA

Figure S5, related to Figure 1 and section Discussion. *The N-terminal segment and the TPR domain of PknG.* (A) PknG (left panel, yellow surface) contains a P-rich region in its N-terminal tail which closely resembles the P-rich region in the C-terminal extension on protein kinasa A (right panel, pink surface). The proline residues involved in each case are shown in sticks. (B) Structure 2PZI shows a series of interactions between the C-terminal portion of the PknG N-terminal segment (gray ribbons and C atoms), the C-terminus of the catalytic core (yellow ribbons and C atoms) and the linker connecting the kinase C-lobe and the TPR domain (green ribbons and C atoms), whose conformation is determined by interaction with the concave surface of the TPR domain. These interactions contribute to stabilize a hairpin encompassing residues 75-78 (GGGL) by leading L_{78} to establish van der Waals contacts with L_{396} (kinase C-lobe) and the aliphatic portions of R_{397} (kinase C-lobe) and R_{408} (linker connecting the kinase C-lobe and the TPR domain). N and O atoms are colored in blue and red, respectively.

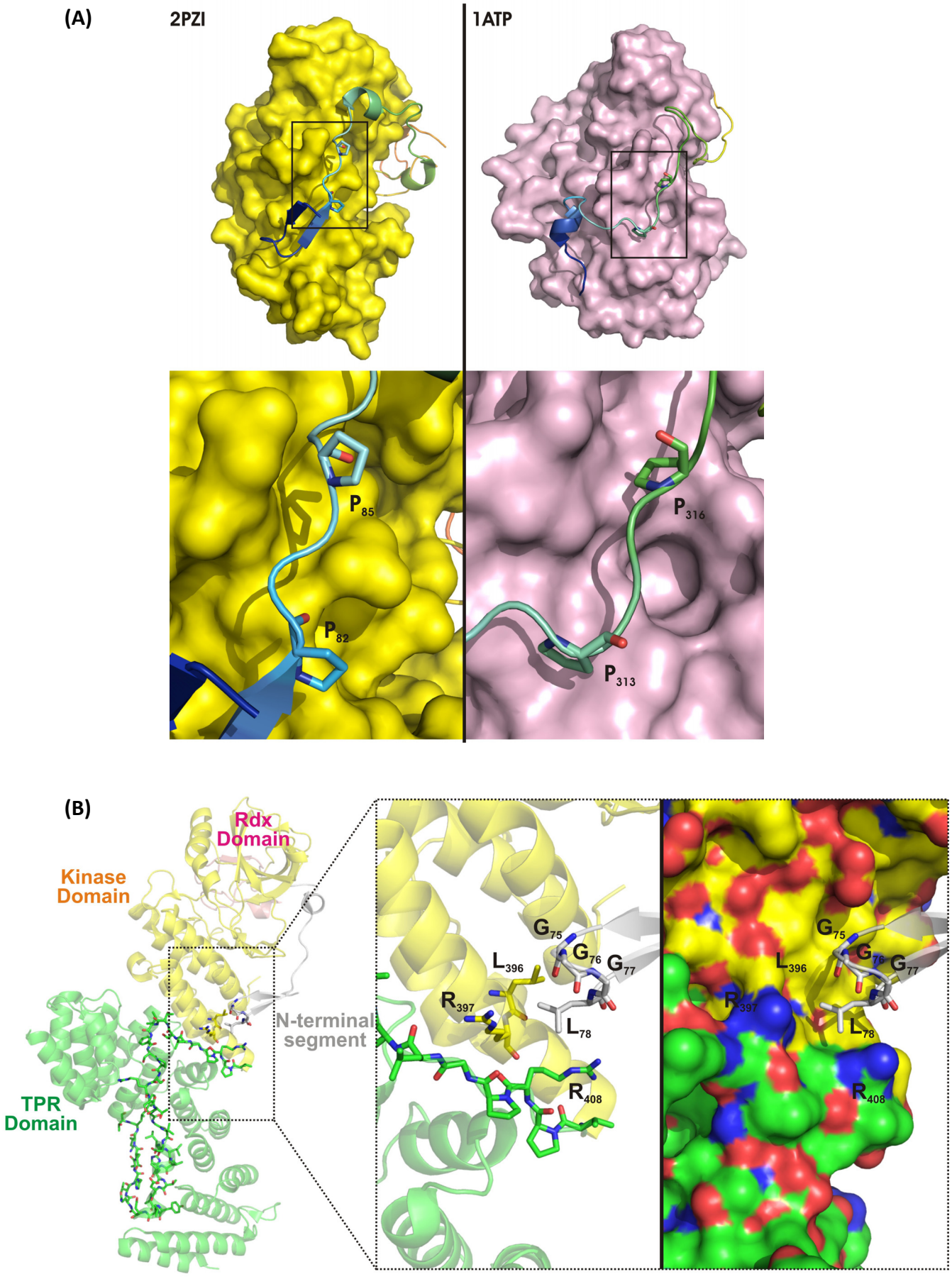
(A)
2PZI
1ATP
P85
P82
P316
P313
(B)
Rdx Domain
Kinase Domain
TPR Domain
N-terminal segment
G75
G76
G77
L396
R397
L78
R408

SUPPLEMENTAL EXPERIMENTAL PROCEDURES

Chemicals

The synthetic 17-mer peptide SDEVTVET$_{21}$TSVFRADFL, corresponding to residues 14-30 of the protein GarA, was produced with a purity >98% by Thermo Fisher Scientific.

Cloning and mutagenesis

Plasmid pET28a-PknG$_{\Delta TPR}$ was generated by site directed mutagenesis of pET28a-PknG, using a pair of complementary primers to introduce a stop codon at position 406 of PknG sequence. Plasmid pET28a-PknG$_{\Delta 137}$, for the expression of the mutant with a hexahistidine tag, was constructed by PCR amplification of *pknG* region 138-750 from vector pET28a-PknG, digestion and ligation into the EcoRI site of plasmid pET28a (Novagen). Plasmid pET28a-PknG$_{E198A}$ was generated by site directed mutagenesis of pET28a-PknG, employing a pair of complementary primers to encode the desired mutation. The oligonucleotides employed are:

ΔTPR-F:	GTCGCCCAGGACACCGGGTAACCGCGGCCAGGGCTATC
ΔTPR-R:	GATAGCCCTGGCCGCGGTTACCCGGTGTCCTGGGCGAC
Δ137-F:	ATTATCATATGGAGAATCTTTATTTTCAAGGTCTGCCGCAGCTAAATCCCG
Δ137-R:	ATTAGGAATTCTTAGAACGTGCTGGT
E$_{198}$A-F:	CAGGCAATGGCGATGGCCGCTCGCCAGTTCCTGGCCGAGGTGG
E$_{198}$A-R:	CCACCTCGGCCAGGAACTGGCGAGCGGCCATCGCCATTGCCTG

Protein production and purification

Wild type PknG and PknG$_{E198A}$ were expressed for 18 h at 30ºC without IPTG. PknG$_{\Delta 73}$ was expressed after 18 h induction at 14ºC with 100 µM IPTG. PknG$_{\Delta 137}$, PknG$_{\Delta TPR}$, PknG$_{\Delta 73,\Delta TPR}$, PknG$_{\Delta 73,\Delta TPR,E\mathbf{T}TS}$ and PknG$_{\Delta 73,\Delta TPR,E\mathbf{A}TS}$ were produced similarly but employing 1mM IPTG. All the proteins were then purified following the same protocol. *E. coli* cells were harvested by centrifugation, re-suspended in lysis buffer (25 mM Hepes, 500 mM NaCl, 20% glycerol, 20 mM imidazole, pH 8) supplemented with Complete protease inhibitor cocktail (Roche) and sonicated. After clarification by centrifugation, the supernatant was loaded onto a 5 ml HisTrap HP column (GE

Healthcare) equilibrated with lysis buffer and the His-tagged protein was then purified applying a linear imidazole gradient (20–500 mM). The PknG-containing fractions, as verified by SDS-PAGE, were pooled and the protein was further purified by size-exclusion chromatography on a Superdex 200 column (GE Healthcare) equilibrated in either 50 mM Tris-HCl, 250 mM NaCl, 5% glycerol, pH 8 (wild type PknG and $PknG_{E198A}$) or 50 mM Tris-HCl, 500 mM NaCl, 5% glycerol, pH 8 (truncated PknG variants). $PknG_{\Delta 137}$ was also prepared adding an additional purification step. Prior to the size-exclusion chromatography, the H_6 tag in $PknG_{\Delta 137}$ was removed by incubating for 18 hours at 18ºC in the presence of His_6-tagged TEV protease at a 1/30 ratio (w/w) in buffer 50 mM Tris-HCl, 500 mM NaCl, 5% glycerol, 1 mM DTT, pH 8, followed by separation on a Ni-NTA agarose column (Qiagen). This step was omitted for the other PknG variants in order to avoid the contact of the protein with DTT (required for TEV activity), which might perturb the metal binding site in the Rdx domain.

Following the purification step by size-exclusion chromatography, fractions corresponding to the PknG peak, as confirmed by SDS-PAGE, were pooled and concentrated up to 30 mg/ml, flash-frozen in liquid nitrogen and stored at -80ºC.

Proteins were quantified by using the molar absorption coefficient predicted from the aminoacid sequence by the ProtParam tool (http://web.expasy.org/protparam/).

Electronic absorption spectroscopy

Electronic absorption spectra were recorded by employing a Beckman Coulter Du 800 spectrophotometer operating at room temperature.

Analytical ultracentrifugation

Sedimentation velocity experiments were carried out at 20 °C in an XL-I analytical ultracentrifuge (Beckman Coulter). Samples were spun using an An60Ti rotor and 12-mm double sector epoxy centerpieces. The partial specific volume of PknG (0.732 $ml \cdot g^{-1}$) was estimated from their amino acid sequences using the software Sednterp. The same software was used to estimate the buffer viscosity (η = 1.032 centipoises) and density (ρ = 1.009 $g \cdot ml^{-1}$). PknG (400 µl at 1 mg/ml) was spun at 42,000 rpm, and

absorbance profiles were recorded every five minutes. Sedimentation coefficient distributions, c(s), were determined using the software Sedfit 14.1 (Schuck, 2000).

Mass spectrometry analysis

The autophosphorylation activity of $PknG_{\Delta 73,\Delta TPR}$, $PknG_{\Delta 73,\Delta TPR,ETTS}$ and $PknG_{\Delta 73,\Delta TPR,EATS}$ was assessed by mass spectrometry after incubation of the different PknG constructs in the presence of 2 mM $MnCl_2$ and 500 µM ATP for 30 min at 37ºC. Protein samples were digested with different proteolytic enzymes (sequencing grade trypsin and endoproteinase GluC from Promega and Roche, respectively) by overnight incubation at 37ºC. Peptides were separated in a reversed-phase column (PepMap RSLC, C18, 75 µm x 500 mm, Thermo) using a linear gradient of B (from 5 to 55%), in 70 min, at 250 nl/min (solvent A: 0.1 % formic acid in H_20; solvent B: 0.1 % formic acid in acetonitrile).

On line mass spectrometry analysis of peptides was performed using a linear ion trap mass spectrometer (LTQ Velos, Thermo) in data dependent acquisition mode (full scan followed by MS/MS of the top 10 peaks in each segment, using a dynamic exclusion list). Raw MS/MS spectra were interpreted with the Proteome Discoverer software package (v.1.3.0.339, Thermo) using Sequest as search engine. The following parameters were used for searching: *Escherichia coli* (strain K12) reference proteome database (Uniprot_2014-12, 4.305 sequences) with the sequences of PknG constructs incorporated; peptide tolerance: 1.5 Da; MS/MS tolerance: 0.8 Da; methionine oxidation and Ser/Thr phosphorylation as allowed variable modifications. Phosphopeptide validation and phosporylation site identification were performed using the PhosphoRS algorithm.

Molecular modeling

In the crystal structures of $PknG_{\Delta 73,\Delta TPR}$, the segment encompassing residues 83-89 (RAPDIDP) of the single PknG molecule within the asymmetric unit gets into the active site of a crystallographic symmetry mate. From this structure, the complex composed by one molecule of PknG plus the fragment RAPDIDP from the symmetry mate was retrieved in order to evaluate their binding. Also, the fragment RAPDIDP provided the starting coordinates for its *in silico* mutation into TVETTSV, corresponding to GarA residues 18-24 and containing the residue T_{21} phosphorylatable by PknG. Binding was

evaluated for the two peptides after energy optimization of complexes $PknG_{\Delta 73,\Delta TPR}$/RAPDIDP and $PknG_{\Delta 73,\Delta TPR}$/TVETTSV by using CHARMM implemented in Discovery Studio 2.5© (Brooks et al., 2009) with the following protocol: 10,000 iterations using Conjugate Gradient algorithm, constraints on the protein backbone, ATPγS, water molecules and cations, no constraint on the peptide and 0.01 RMS gradient as stop criterion. The total potential energy and the binding energy between the protein and the peptide were calculated for each complex.

SUPPLEMENTAL REFERENCE LIST

Bonomi,F., Iametti,S., Kurtz,J., Richie,K.A., and Ragg,E. (1998). Direct metal ion substitution at the [M(SCys)4]2− site of rubredoxin. JBIC *3*, 595-605.

Brooks,B.R. et al (2009). CHARMM: the biomolecular simulation program. J. Comput. Chem. *30*, 1545-1614.

Schuck,P. (2000). Size-distribution analysis of macromolecules by sedimentation velocity ultracentrifugation and lamm equation modeling. Biophys. J. *78*, 1606-1619.

Sieker,L.C., Stenkamp,R.E., and LeGall,J. (1994). Rubredoxin in crystalline state. Methods Enzymol. *243*, 203-216.